Article:

Woodhouse, A, Barnes, PM, Shorrock, A et al. (17 more authors) (2022) Trench floor depositional response to glacio-eustatic changes over the last 45 ka, northern Hikurangi subduction margin, New Zealand. New Zealand Journal of Geology and Geophysics. ISSN 0028-8306

https://doi.org/10.1080/00288306.2022.2099432

Trench floor depositional response to glacio-eustatic changes over the last 45 ka, northern Hikurangi subduction margin, New Zealand

Adam Woodhouse[1,2], Philip M. Barnes[3], Anthony Shorrock[4], Lorna J. Strachan[4], Martin Crundwell[5], Helen C. Bostock[3,6], Jenni Hopkins[7], Steffen Kutterolf[8], Katharina Pank[8], Erik Behrens[3], Annika Greve[9], Rebecca Bell[10], Ann Cook[11], Katerina Petronotis[12], Leah LeVay[12], Robert A. Jamieson[1], Tracy Aze[1], Laura Wallace[2,5], Demian Saffer[2], Ingo Pecher[4,13]

[1]University of Leeds, Leeds, UK.

[2]University of Texas Institute for Geophysics, Austin, TX, USA.

[3] National Institute of Water and Atmospheric Research, Wellington, New Zealand.

[4] University of Auckland, Auckland, New Zealand.

[5]GNS Science, Lower Hutt, New Zealand.

[6]University of Queensland, Brisbane, Australia.

[7]Victoria University of Wellington, Wellington, New Zealand.

[8]GEOMAR Helmholtz Centre for Ocean Research Kiel, Kiel, Germany.

[9]Utrecht University, Utrecht, The Netherlands.

[10]Imperial College London, London, UK.

[11]The Ohio State University, Columbus, OH, USA.

[12]Texas A&M University, College Station, TX, USA.

[13]Texas A&M University – Corpus Christi, Corpus Christi, TX, USA

Correspondence address: Dr Adam Woodhouse, University of Texas Institute for Geophysics, J.J. Pickle Research Campus, University of Texas at Austin, Austin, Texas, United States of America

Correspondence email: adam.woodhouse@austin.utexas.edu

ABSTRACT

Glacio-eustatic cycles lead to changes in sedimentation on all types of continental margins. There is, however, a paucity of sedimentation rate data over eustatic sea-level cycles in active subduction zones. During International Ocean Discovery Program Expedition 375, coring of the upper ~110 m of the northern Hikurangi Trough Site U1520 recovered a turbidite-dominated succession deposited during the last ~45 kyrs (Marine Isotope Stages (MIS) 1-3). We present an age model integrating radiocarbon dates, tephrochronology, and $\delta^{18}O$ stratigraphy, to evaluate the bed recurrence interval (RI) and sediment accumulation rate (SAR). Our analyses indicate mean bed RI varies from ~322 yrs in MIS1, ~49 yrs in MIS2, and ~231 yrs in MIS3. Large (6-fold) and abrupt variations in SAR are recorded across MIS transitions, with rates of up to ~10 m/kyr occurring during the Last Glacial Maximum (LGM), and <1 m/kyr during MIS1 and 3. The pronounced variability in SAR, with extremely high rates during the LGM, even for a subduction zone, are the result of changes in regional sediment supply associated with climate-driven changes in terrestrial catchment erosion, and critical thresholds of eustatic sea-level change altering the degree of sediment bypassing the continental shelf and slope via submarine canyon systems.

Introduction

Subduction trenches can vary greatly in their dimensions and sedimentary fill (Jarrad, 1986; Underwood and Moore, 1995), where lithologies, facies architecture, total thickness, and depositional rates of trench sediments are strongly controlled by climate, sedimentary dynamics, tectonic-geomorphology of the margin, plate convergence rate, and uplift rates in detrital source areas (von Huene, 1974; Schweller and Kulm, 1978; Underwood and Bachman, 1982; Underwood, 2007). In trench settings characterised by relatively high rates of siliciclastic sedimentation (>1 m/kyr), sediment thickness can exceed 7 km (e.g., Westbrook et al. 1984; Smith et al. 2012; McNeill and Henstock, 2014). Terrigenous sediments are predominantly delivered to trenches via transverse submarine canyons and slope gullies that cut across or circumvent bathymetric obstructions such as structural ridges (Underwood and Karig, 1980; Thornburg et al. 1990; Lewis et al. 1998; Völker et al. 2006; Bourget et al. 2011; Goldfinger et al. 2012). Transport parallel to the margin also occurs through axial channels (Piper et al. 1973; Thornburg and Kulm, 1987; Covault et al. 2012; McArthur and Tek, 2021) and through reworking or sustained suspension by bottom currents (Carter and McCave, 1994).

Sediment cores recovered during half a century of ocean drilling and shallow (<30 m depth) gravity/piston coring show that trench facies in siliciclastic settings are dominated by gravity-flow deposits with varied proportions of hemipelagite and tephra (e.g., Piper et al. 1973; Aubouin et al. 1982a, b; Taira and Niitsuma, 1985; Kimura et al. 1997; Westbrook et al. 1994; Underwood and Moore, 1995; Nelson et al. 2000a; Moore et al. 2001; Underwood, 2007; Harris et al. 2013; Jaeger et al. 2014; Barnes et al. 2019). Typical sediment accumulation rates (SAR) range from 0.2 to >1.5 m/kyr, and temporal variability in those rates may be affected by numerous factors including tectonic uplift of detrital source area, progressive deformation of the accretionary prism, seismicity, volcanism, changes in climate and eustatic sea-level, and anthropogenic landscape modification (von Huene and Kulm, 1973; Nelson, 1976; Underwood and Karig, 1980; Underwood and Moore, 1995; Völker et al. 2006; Covault and Graham, 2010; Goldfinger et al. 2012; Pouderoux et al. 2012a; Harris and Whiteway, 2011; Bourget et al. 2011; Kuehl et al. 2016; Soutter et al. 2021). These studies indicate that gravity flow deposits are commonly emplaced with decadal to multi-century recurrence intervals (RIs). Furthermore, one of the key considerations may be the spacing of submarine canyons along the strike-length of the margin, and their proximity to the shoreline over the course of full eustatic cycles (e.g., Bourget et al. 2010).

Quantitative data on sedimentation rates and turbidite RIs in trenches at timeframes of 10^4 yrs are sparse, although several studies present age models of sequences spanning timeframes of several tens of thousands of years (e.g., Zuffa et al. 2000; Underwood et al. 2005; Blumberg et al. 2008; Knudson and Hendy, 2009; Bourget et al. 2010). Consequently, although the general spatio-temporal depositional settings are well-studied, accurate documentation of how individual trench sequences respond to high-order glacio-eustatic sea-level cyclicity is currently limited.

In this study, we use a Late Pleistocene-Holocene aged succession at Site U1520 from the northern Hikurangi Trough, eastern New Zealand, cored during International Ocean Discovery Program (IODP) Expedition 375 (Fig. 1) (Wallace et al. 2019a; Barnes et al. 2019). Our analysis provides a high-resolution assessment of trench-floor sedimentation at this site over the last ~45 ka spanning major glacio-eustatic sea-level cyclicity. We quantify the magnitude and interpret the major causes of changes in SAR, as well as comparing our results with core data from other subduction trenches spanning similar timeframes.

Regional Subduction Setting and Location of Site U1520

The Hikurangi Subduction Margin (HSM) straddles the boundary between the obliquely converging Australian and Pacific plates (Fig. 1; Wallace et al. 2004). The margin strikes NNE-SSW and extends ~750 km from NE South Island to the southern Kermadec Trench (Lewis and Pettinga, 1993; Wallace et al. 2009; Barnes et al. 2010).

The Hikurangi Trough is a sediment-rich subduction system, with onlapping trench-wedge sediments (Underwood and Moore, 1995) ranging in thickness from ~6 km in the south to <1 km in the north (Lewis et al. 1998; Plaza-Faverola et al. 2012; Ghisetti et al. 2016; Barnes et al. 2019, 2020; McArthur et al. 2020). Sediment is delivered by >10 shelf-incising canyons and numerous submarine slope gullies (e.g., Lewis and Barnes, 1999; Orpin, 2004; Mountjoy et al. 2009, 2013; Pedley et al. 2010; Watson et al. 2020). Axial sediment transport is focussed through the Hikurangi Channel, which traverses the trench for >600 km before turning sharply eastward to cross the oceanic Hikurangi Plateau (Figs. 1 and 2A) (Lewis, 1994; Lewis et al. 1998; Lewis and Pantin, 2002, Mountjoy et al. 2018; McArthur and Tek, 2021; Tek et al. 2021a, b).

Hikurangi Trough terrigenous sediments are sourced from both the South (today primarily from Kaikōura and Cook Strait canyons) and North islands (including Madden and Māhia canyons), with rates fluctuating significantly over glacial-interglacial cycles (Lewis et al. 1998; Lewis and Barnes, 1999; Berryman et al. 2000; Eden et al. 2001; Carter and Manighetti, 2006; Carter et al. 2008; Alloway et al. 2007; Mountjoy et al. 2009, 2013; Pouderoux et al. 2012a; Barrell, 2013; Upton et al. 2013; Claussmann et al. 2021, 2022). Furthermore, large earthquakes (M_W >7.0), internal tides, and storm-associated hyperpycnal flows can trigger turbidity currents, debris flows, and slumps, reworking and transporting large amounts of sediment to the trough (Pouderoux et al. 2012b; Kuehl et al. 2016; Mountjoy et al. 2018, 2020; Howarth et al. 2021). Dispersal offshore has occurred via a range of processes including downslope gravity flows (e.g., Lewis et al. 1998; Lewis and Barnes 1999; Lewis and Pantin, 2002; Orpin 2004; Pouderoux et al. 2012a; Mountjoy et al. 2013, 2018; Watson et al. 2020; Howarth et al. 2021; Tek et al. 2021a, b) and alongslope oceanic currents (e.g., Carter and Manighetti, 2006; Paquet et al. 2009; Bostock et al. 2019a, b; Bailey et al. 2021; Tek et al. 2021a, b).

There is also air-fall deposition of tephra, dominantly sourced from explosive eruptions within the Taupō Volcanic Zone (TVZ) of the central North Island (Fig. 1) (e.g., Carter et al. 1995, 2002; Hopkins et al. 2021a, b).

IODP Site U1520 is located in the northern Hikurangi Trough in ~3520 m water depth, 16 km east of the deformation front (Barnes et al. 2019). Here the forearc wedge is ~70 km wide and exhibits mixed frontal accretion and tectonic erosion in response to subducting seamounts (Collot et al. 1996, 2001; Lewis et al. 1998; Pedley et al. 2010; Bell et al. 2010; Barker et al. 2018; Gray et al. 2019; Barnes et al. 2020; Gase et al. 2021). The trough sedimentary succession varies in thickness from ~1-0.5 km and pinches out seaward against incoming seamounts (Figs. 1 and 2) (Lewis et al. 1998; Barnes et al. 2019, 2020; Gase et al. 2021). Site U1520 is positioned between the subduction deformation front and the volcanic Tūranganui Knoll (Figs 1 and 2; Barnes et al. 2019), which rises ~1000 m above the trench floor. To the northeast lies the broad, flat, Whenuanuipapa Plain and Ruatoria Debris Avalanche (Lewis et al. 1998, Collot et al. 2001). To the south, a prominent field of sediment waves occurs between Tūranganui Knoll and the mouth of Māhia Canyon (Lewis et al. 1998; Pedley et al. 2010, Shorrock, 2021).

IODP drilling at Site U1520 recovered a ~1 km thick sediment succession (Fig. 2B; Barnes et al. 2019). Here we focus on the uppermost stratigraphic unit as defined by shipboard scientists, Unit I (see Supplementary Information (SI); Barnes et al. 2019), which extends from 0-110 metres below seafloor (mbsf). Unit I is comprised predominantly of silts and sands with minor clay and tephra, accumulated over the last ~45 kyrs, with sedimentary structures indicative of multiple depositional processes.

Regional Oceanography

East coast New Zealand waters are influenced by the complex interplay of several water masses, eddies, currents, and fronts (Fig. 1). The shelf and upper slope of the eastern North Island is bathed in warm, salty, nutrient-poor subtropical waters (STW) associated with the East Auckland Current (EAUC) and East Cape Current (ECC) (Fig. 1; Chiswell et al. 2015; Lorrey and Bostock, 2017; Stevens et al. 2021). The ECC transports water southwest offshore of the North Island at water depths down to ~2000 metres (Fig. 1) (Chiswell, 2005; Chiswell et al. 2015), influencing sediment transport and deposition along the continental slope (Carter and Manighetti, 2006; Carter et al. 2010; Keuhl et al. 2016; McArthur et al. 2020; Bailey et al. 2021). Reported flow speeds vary with depth; ~0.25 ms^{-1} at 100 mbsl, decreasing to 0.10 ms^{-1} at 1000 mbsl (Carter et al. 2002).

Inshore of the ECC, the continental shelf is influenced by cool, low salinity, nutrient-rich surface water of the Wairarapa Coastal Current (WCC) flowing to the northeast (Figs. 1 and 2A) (Brodie, 1960; Chiswell, 2000). The WCC is a combination of Subantarctic Surface Water (Heath, 1975; Sutton, 2003), and STW transported by the D'Urville Current (dUC) through Cook Strait (Fig. 1). Nearshore swell waves, wind direction, and the northward flowing WCC with ephemeral gyres, primarily associated with the ECC, control sediment transport dynamics (Foster and Carter, 1997; Chiswell, 2000).

Deep-water currents east of New Zealand comprise the Deep Western Boundary Current (DWBC), which flows into the Pacific Ocean around the Chatham Rise (Carter and McCave, 1994; Whitworth et al. 1999), and consists of Lower Circumpolar Deep Waters (LCDW) flowing at water depths >2500 mbsl (Chiswell et al. 2015; Lorrey and Bostock, 2017). Below ~3500 mbsl, the LCDW is steered along the eastern edge of the Hikurangi Plateau, interacting with seafloor morphology before flowing north along the

Kermadec Trench slope (Fig. 1) (Fenner et al. 1992; Carter and McCave, 1994; McCave and Carter, 1997; Moore and Wilkin, 1998; Whitworth et al. 1999; Chiswell et al. 2015). The velocity of deep-water flow on the floor of the northern Hikurangi Trough is unknown as instrumented observations are yet to be recorded.

Oceanic currents are inferred to influence sediment dispersal and deposition on the Hikurangi trench floor (Lewis and Pantin, 2002; Carter and Manighetti, 2006; Bailey et al. 2020, 2021) and across contourite drifts of the Hikurangi Plateau (Fenner et al. 1992; Carter and McCave, 1994; McCave and Carter, 1997; Saffer et al. 2019). Previous paleoceanographic studies indicate that during the Last Glacial Maximum (LGM; see Clark et al. 2009) the strength of the ECC decreased, while the proto-Wairarapa Coastal Current (pWCC) strengthened (Carter and Manighetti, 2006). In the deep waters of the Hikurangi Plateau, analysis of sortable silt fractions at core site CHAT 10K (Fig. 2A) (3003 mbsl, McCave et al. 2008) reveal little sedimentological change between the Holocene and the LGM, potentially indicating similar bottom-current activity was sustained across the eastern Hikurangi Plateau.

Materials and Methods

Sedimentological Analyses

Lithological descriptions of Unit I integrate high-resolution core line-scan images, Gamma Ray Attenuation (GRA) bulk density (Wetzel and Balson, 1992; Goldfinger et al. 2012), computed tomography (CT) numbers (Mees et al. 2003; Reilly et al. 2017; Vandekerkhove et al. 2020) and laser grain-size measurements (Shorrock, 2021). We use these data to identify sedimentary structures and bed types (Figs. S1 and S2), allowing us to develop bed thickness and frequency statistics (see SI).

We conducted high resolution (~0.01 m spacing) laser grain-size measurements of two short (<50 cm) u-channel sub-cores, using a Beckman Coulter LS 13 320 Laser Diffraction Particle Size Analyser at the National Institute of Water and Atmospheric Research (NIWA) (see SI; Table S2; Fig. S2). These grain-size data were calibrated against GRA bulk densities, so that grain-size could be inferred using GRA as a proxy. Bedforms are characterised following Ashley (1990) and Baas et al. (2016).

Tephra Analysis

Bulk sediment samples of tephra were wet sieved, isolating the 63-250 μm size fraction to concentrate glass shards. These were then mounted on acrylic tablets, polished to reveal fresh shard faces, and carbon coated for geochemical analysis at GEOMAR with the JEOL JXA 8200 Electron Microprobe Analyser (SI; Figs. S3 and S4). The tephra deposits were correlated geochemically to known marker horizons using reference material from the TephraNZ database (Hopkins et al. 2021a, b).

Foraminiferal Analyses

Samples from close to volcanic tephra and from fine-grained muddy facies were selected for radiocarbon dating (^{14}C). At least 200 specimens per sample of planktonic foraminifera (*Globoconella inflata*) were handpicked from the 212-500 μm size fraction, cleaned, and assessed under light microscope for preservation quality (e.g., Sexton et al. 2006; Edgar et al. 2015). These were analysed for ^{14}C using the modified compact Accelerator Mass Spectrometer at the Rafter Radiocarbon Laboratory, GNS Science (Table S3; see SI for calibration details). For assemblage analysis, sediments were sieved to >150 μm and split to fractions containing 300-600 foraminifera specimens for identification. Planktonic and benthic foraminiferal assemblages were identified to provide information on biostratigraphy, paleoceanography (Crundwell et al. 2008;

Crundwell and Woodhouse, 2022, Submitted), oceanicity (greater planktonic % corresponds to greater oceanicity; Hayward et al. 1999, 2001), and paleo-water depth (key benthic species; Crundwell et al. 1994; Hayward et al. 2010; 2019) (Table S4). For stable $\delta^{18}O$ and $\delta^{13}C$ isotope analysis, where present, well-preserved planktonic (*Neogloboquadrina incompta*) and benthic foraminifera (*Uvigerina peregrina*) were picked from the >212 μm fraction and analysed using the Isoprime Dual-Inlet Isotope Ratio Mass Spectrometer at the University of Leeds, UK (Table S4).

Age Modelling

An age-depth model with 1 and 2 sigma uncertainties was constructed from calibrated radiocarbon dates and tephra ages (see SI for details, Fig. S5; Table S5) using the software "*Undatable",* which is well suited for Unit I deposits (Lougheed and Obrochta, 2019). Based on the median age model we calculated the sediment accumulation rate (SAR) and the bed recurrence interval (RI, number of beds/age interval).

Numerical Modelling of Bottom Currents

Bottom currents and their variance at Site U1520 were extracted from an existing eddy resolving (1/20 degree) ocean model hindcast (Behrens et al. 2021, SI for details) over the New Zealand region, to assess the influence of currents on sedimentation.

Results and Interpretations

Core Lithostratigraphy

The Unit I succession is dominantly siliciclastic, composed of silt, with variable mixtures of accompanying sand and clay (Figs. S1 and S2). Unit I is also intercalated with rare centimetre- to decimetre-thick tephras (e.g., Fig. 3; see SI).

A wide variety of well-defined bed types were observed with sharp upper and lower contacts that often truncate physical and biogenic sedimentary structures (Shorrock, 2021), along with thin laminae. Many follow a similar vertical grain-size motif, broadly defined as normally graded bi-partite silt-rich beds (*sensu* Stevenson et al. 2014) with a lower, coarser-grained, well-sorted interval (dominantly silty and including rare pebbly sand and sands) overlain by a finer grained, moderately- to poorly-sorted upper interval (silts and clays; Fig. 3, Fig. S2). Other vertical grain-size profiles are observed, including inverse-graded, non-graded, and complex grading patterns (Fig. 3; see Strachan et al. 2016). The lower intervals of beds are commonly black or grey, except in the upper 0-10 mbsf where they are dark olive green (Fig. 3). Lower intervals preserve a diverse range of structures including parallel laminae, wavy laminae with well-preserved ripple-forms as well as low-angle and dune-scale cross-beds, mesoscale banding (*sensu* Lowe and Guy, 2000), scours, convolutions, soft-sediment folding, dewatering structures, and sub-angular silt clasts (Fig. 3). The upper silt-clay intervals of beds are light olive green, and either non-graded or normally graded. Upper intervals have a range of observed sedimentary structures including parallel and inclined laminae, intra-laminae flame and load casts, and laminated convolutions. Well defined macroscale bioturbation is commonly observed in the upper parts of beds in the upper interval from 0-10 mbsf, (Fig. 3A), becoming less common below 10 mbsf.

We identify 605 beds within Unit I, with a mean bed thickness of 0.16 m, and minimum and maximum values of 0.01 and 6.39 m, respectively. These figures differ slightly from the shipboard bed statistics of Barnes et al. (2019) (see SI). Bed frequency varies down core with 4-6 beds per m (bpm) in the 0-6.5 mbsf interval, 4-10 bpm from 6.5-10 mbsf, 1-13 bpm between 10-56 mbsf, 0-10 bpm from 56-92 mbsf, and 3-15 bpm between 92-106 mbsf (Fig. 4).

Interpretation:

The dominant stacked bi-partite beds bounded by distinct truncating upper and lower contacts are interpreted as deposits of single depositional events due to: 1) the gradational transition between lower and upper intervals; 2) the continuity of laminae and bands across intervals; and 3) the lack of evidence for erosion or depositional hiatuses across internal boundaries (Fig. 3). The wide range of physical sedimentary structures in lower and upper bed intervals indicate that the dominant mode of deposition was via grain-by-grain aggradation associated with unidirectional, tractional turbidity currents (*sensu* Kneller and Buckee, 2000). The bi-partite event beds are interpreted as being deposited from flows with variable rheologies and particle support mechanisms including high to low-density fine-grained turbidity currents (*sensu* Piper, 1978; Stow and Shanmugam, 1980; Stow and Piper, 1984; Strachan et al. 2016) and transitional flows (*sensu* Haughton et al. 2009; Baas et al. 2011; 2016). Vertical grading profiles in lower intervals imply a range of temporal behaviours including dominantly waning flows (normally graded), and less common waxing (inverse-graded), steady (non-graded), and unsteady flows (variably graded) (e.g., Kneller, 1995; Ho et al. 2018). The presence of parallel and inclined laminae in upper intervals indicates deposition of upper stage plane beds and ripples, and therefore implies that flows had a high velocity, but became muddier with time (e.g., Stevenson et al. 2020). In addition, common dewatering structures imply either syn-depositional loading by rapidly deposited flow tails, or dewatering triggered by the next event. These observations reveal a succession dominated by stacked gravity flow deposits including turbidites (*sensu* Bouma, 1962; Piper, 1978; Lowe, 1982; Stow and Shanmugam, 1980; Talling et al. 2012), hybrid event beds (*sensu* Haughton et al. 2009), potential hyperpycnites (*sensu* Mulder et al. 2003), debrites (*sensu* Iverson, 2005), and slumps (Stow, 1982) (see SI for details). Based on the preserved physical sedimentary structures and bedding contacts in the upper bed throughout Unit I, they are considered here to be primarily associated with tractional deposition from muddy gravity flows or modified mixed turbidite-contourite deposition (Gong et al. 2018), and not from pure hemipelagic deposition. This interpretation contrasts with Pouderoux et al. (2012a), Barnes et al. (2019), and Noda et al. (Submitted), who inferred the preservation of significant hemipelagic deposition between gravity flow deposits.

Bioturbation in the upper parts of beds, between 0-10 mbsf, indicates that prevailing seafloor conditions had sufficient oxygen, nutrients, and heat (Kao et al. 2010) for organisms to colonise and live within the upper seafloor substrate, suggesting consistent re-colonization following turbidity current deposition. Similar bioturbation patterns have been observed elsewhere on the HSM in Holocene strata (Carter et al. 2002; Manighetti et al. 2003; Campbell et al. 2010; Pouderoux et al. 2012a), including following the 2016 Kaikōura co-seismic turbidite, which showed evidence of recolonization ~8 months after emplacement (Howarth et al. 2021). The source of oxygen-rich bottom waters with abundant food is open to debate and may be attributed to the turbidity currents themselves (e.g., Kane et al. 2007) or moving regional water masses (Carter et al. 2002; Chiswell et al. 2015). The dramatic reduction of biogenic traces beneath 10 mbsf implies a deterioration in suitable conditions during deposition.

Radiocarbon and Tephra Chronology

We measured eight AMS-^{14}C radiocarbon ages from Unit I (Table 1). The shallowest ^{14}C sample from 5.25 mbsf produced a calibrated median age of 8695 yrs BP, and the deepest from 106.26 mbsf, an age of 42,440 yrs BP (Table 1; Fig. 4).

Seventeen macroscopic tephras were identified and sampled from Unit I, positioned between ~0-30 mbsf (Fig. 4). All tephra samples show discrete, homogenous glass chemistries, representing eight eruptions, five of which are correlated geochemically and stratigraphically to well-known large rhyolitic marker horizons from the reference material from the TephraNZ database (Table 2; Figs. S3 and S4; Hopkins et al. 2021a, b). For the andesitic, dacitic, and trachytic samples, the geochemical correlation is more complicated due to the homogeneity of potential source material, and the lack of suitable reference data (Figs. S3 and S4). As a result of these ambiguities, these tephras were not used in the construction of the integrated age model.

Interpretations:

Whilst foraminifera were picked from fine-grained lithofacies, some of the dated material is likely to be reworked in turbidites and may therefore provide upper depositional ages. Nevertheless, the radiocarbon dates show an increase in age down core with no age reversals. Furthermore, the dates agree with the rhyolitic tephra ages, correlated to their terrestrial counterparts including the Taupō (1.7 ka), Waimihia (3.4 ka), Whakatane (5.5 ka), Rotoma (9.4 ka), and Opepe eruptions (9.9 ka; Table 2).

Age Modelling, Sediment Accumulation Rates, and Bed Recurrence Intervals

Age models were developed using the tephrochronology and radiocarbon ages, to provide chronostratigraphy for Unit I (Fig. 4). Unit I shows a continuous age model down to ~45 ka (Tables 1 and 2). Calculated age confidence ranges increase with depth from <2 kyrs in the upper few metres to ~12 kyrs towards the base of the Unit I (see SI). The good agreement between radiocarbon dates and rhyolitic tephra ages indicates that dating of reworked foraminifera in muddy turbidites has not had a significant impact on the age model.

The age model reveals a median sediment accumulation rate (SAR) and median recurrence interval (RI) for emplacement of event beds averaged across the entire Unit I thickness at Site U1520 of ~2.4 m/kyr and 184 yrs, respectively. The mean SAR in the top ~10 mbsf (~14.5 ka) is ~0.86 m/kyr (Fig. 4). This rate increases down-core to ~5 m/kyr from 10-32 mbsf (~14.5-20 ka), and subsequently to ~9 m/kyr between ~32-48 mbsf (~20-21 ka), with a peak of 9.95 m/kyr at 41 mbsf (~20.5 ka). Continuing down core, from ~48-56 mbsf (~21-24 ka), the SAR reduces to ~3 m/kyr, and then increases to ~8 m/kyr from 56-95 mbsf (~24-29 ka). Between 95-106 mbsf (~29-45 ka), the SAR reduces to ~0.8 m/kyr (Fig. 4). Decompaction could potentially increase these linear SAR values by up to 10% (Fig. S6; see SI).

Mean RI from <10 mbsf (<14.5 ka) is ~322 yrs, showing a distinct peak of ~1000 yrs at ~3.6 mbsf (~5 ka). Down-core, from 10-95 mbsf (~14.5-29 ka), the mean RI is substantially reduced to ~49 yrs, remaining low throughout this interval. Values then increase slightly from 95-106 mbsf (~29-45 ka) to ~172 yrs, with a minor peak at ~105 mbsf (~42 ka) of ~500 yrs (Fig. 5).

Interpretation:

The "*Undatable*" age model provides a chronology of the core dating to ~45 ka, indicating that the core covers MIS1-3. The age model errors increase down core due to limited tephra and radiocarbon dates deeper in Unit I, and the likelihood of reworking of dated sediments, particularly in MIS2 (Fig. 6). SARs and RIs are highly variable at Site U1520. SARs range from 0.86 m/kyr during MIS1, and peak at 9.95 m/kyr in the LGM during MIS2, when mean RIs were lowest, whilst MIS3 SARs are similar to MIS1 at 0.8 m/kyr (Fig. 4). This indicates different conditions during the LGM versus deglaciation, resulting in significantly higher SARs and lower RIs.

Foraminiferal Assemblage Data

Planktonic foraminiferal biogeographic groups are dominated by a high abundance of tropical-subtropical taxa at depths of <15 mbsf, whilst through the rest of Unit I (~15-106 mbsf) they are highly variable (Fig. 6). The percentage of planktonic foraminifera from 0-15 mbsf (60-100%) indicate suboceanic-oceanic settings (Fig. 4). They then fluctuate significantly between outer neritic-suboceanic (30-60%) to open oceanic (>90%) at ~15-95 mbsf, below which, suboceanic-oceanic (60-100%) settings are re-established.

Benthic foraminifers indicate sedimentary input from paleo-water depths of 600-1000 mbsl from 0-15 mbsf, 0-200 mbsl from 15-56 mbsf, and large fluctuations between 0-1000 mbsl from 56-106 mbsf (Fig. 4). Sediments from ~15-92 mbsf also show markedly heightened occurrences of Miocene/Pliocene planktonic foraminifera within gravity flow deposits (Crundwell and Woodhouse, Submitted), sometimes accounting for >50% of the total assemblage (Fig. 6).

Interpretations:

Increasing abundances of warm-water taxa at depths of <10 mbsf are consistent with regional deglaciation (Figs. 4 and 6) (Crundwell et al. 2008; Crundwell and Woodhouse, 2022, Submitted). Fluctuating planktonic foraminiferal biogeographic group abundances and ubiquitous Miocene and Pliocene specimens in gravity flows from 15-92 mbsf (Fig. 6; Crundwell and Woodhouse, Submitted) suggest reworking of uplifted sediments on land, or erosion of slope sediments during sea level lowstand (Fig. 2A). This is further supported by the presence of shallow water benthic foraminifera (shelfal to mid-bathyal, 0-1000 m; Hayward et al. 2010, 2019) at Site U1520 (3520 mbsf) providing evidence for the allochthonous nature and downslope transport of the sediment at Site U1520. These data support the above suggestion that some radiocarbon dates provide upper depositional ages.

Foraminifera Isotope Data

Planktonic foraminifera exhibit excellent preservation, where stable isotope $\delta^{18}O$ ($\delta^{18}O_{Planktonic}$) values from ~5-15 mbsf consistently track ~3 ‰ lighter than benthic $\delta^{18}O$ ($\delta^{18}O_{Benthic}$) values (Fig. 4). However, from ~12-15 mbsf, the $\delta^{18}O_{Benthic}$ values become slightly out of phase (Fig. 4). From ~15-95 mbsf, planktonic foraminifera continue to be well-preserved, with $\delta^{18}O_{Planktonic}$ values consistently ~2 ‰. In contrast, benthic foraminifera are rare between ~15-95 mbsf, and when present, exhibit poor preservation with significant deviations from the consistent $\delta^{18}O_{Planktonic}$ signal (Fig. 4). The $\delta^{18}O_{Planktonic}$ signal records a +0.7 ‰ shift at ~93-101 mbsf, stabilizing for the remainder of Unit I (Fig. 4).

Interpretations:

The $\delta^{18}O_{Planktonic}$ values support age modelling data showing a typical oxygen isotope trend for the last glacial to interglacial (Fig. 4). However, $\delta^{18}O_{Benthic}$ values (SI) are inconsistent with the expected Holocene regional water depth signal from LCDW (>2500 mbsl, ~3.1‰) bathing Site U1520 (~3520 mbsl) (Table S4) (McCave et al. 2008), and more comparable to *Uvigerina* spp. bathed by North Pacific Deep Water/Upper Circumpolar Deep Water (~1500-2500 mbsl, ~3.4‰) suggesting transport from shallower bathyal waters (McCave et al. 2008; Lorrey and Bostock, 2017).

Numerical Modelling of Bottom Currents in the Northern Hikurangi Trough

The modelled simulation (see Behrens et al. 2021) produces the strongest bottom currents with largest variance on the continental shelf and upper slope in water depths of <500 m, and over localised ridges on the continental slope in water depths of <1500 m, in the path of the ECC (Figs. 2 and S8). Increased bottom current flows are also simulated around the flanks of seamounts on the subducting northern Hikurangi Plateau, which protrude above the Hikurangi Trough into the path of the DWBC (Figs. S8 and S9). At

Site U1520 the simulation produces mean and maximum bottom flow velocities at 3200 m of ~0.06 ms^{-1} and 0.35 ms^{-1}, respectively, in the path of LCDW (Chiswell et al. 2015).

Interpretations:

The threshold for cohesionless sediment transport and deposition (e.g., critical Shields parameter) is a function of current velocity and specific grain, cohesion and turbulence variables (see review by Yang et al. 2019), but is not well established for cohesive silt and clay particles at grain-sizes of <10-20 μm in which aggregation and flocculation is important (e.g., McCave 1984a, b). Simplified thresholds based on bottom-current velocities and grain-size indicate that currents below 0.10-0.15 ms^{-1} are likely to be associated with deposition of sand and silt, whilst velocities >0.15-0.20 ms^{-1} are required for transport of fine sand (Postma, 1967). The mean simulated current velocity at 3200 mbsl at Site U1520 (~0.06 ms^{-1}; Fig. S9) is therefore unlikely to erode *in situ* silt and fine sand, or to significantly transport silt introduced in the tail of gravity flows. High energy events, and periods of maximum flow velocities of 0.35 ms^{-1} however, may be associated with re- or ongoing- suspension in the benthic boundary layer and erosion of the *in-situ* basin floor cannot be ruled out (e.g., McCave and Hall, 2006). Furthermore, there is no discernible moat around the western flank of Tūranganui Knoll within the vicinity of Site U1520 (Fig. 2B), though drifts and moats have been observed on top of the seamount (Wallace et al. 2019b).

Discussion

Integrated Age Model - IODP Site 1520 Unit I

The sedimentological and paleontological record at Site U1520 allow for the construction of an integrated age model with consistent agreement between dating methodologies (Fig. 4). Despite increasing age confidence ranges with depth (up to ~12 kyr), cross correlation with $\delta^{18}O_{Planktonic}$ values has allowed us to constrain the key MIS boundaries (Fig. 4).

Our age model indicates Unit I comprises Holocene to Late Pleistocene strata, providing a highly expanded ~110 m succession representing the last 45 kyrs (Fig. 4). Despite being dominated by gravity flow deposits containing reworked material (e.g., Toucanne et al. 2008), the core and $\delta^{18}O_{Planktonic}$ record are consistent with tephra chronology and preserve a paleoceanographic record of MIS1 and 2, and the latter part of MIS3 (Fig. 4; Lisiecki and Raymo, 2005).

Trench-floor depositional response to glacio-eustatic change

Here, we discuss changes in lithological character and provenance, sedimentary processes, and sedimentation rates at Site U1520 in relation to glacio-eustatic climatic changes through MIS1-3.

Marine Isotope Stage 1:

The dominance of normally graded, bipartite beds that contain remobilised slope benthic foraminifera in MIS1 strata reveal a depositional system dominated by downslope gravity flows sourced from 600-1000 mbsl (Fig. 4). A total of 59 beds, with typical thicknesses of 15-25 cm, are identified within the MIS1 interval.

MIS1 strata are unique within Unit I for two reasons: first, lower bed intervals are distinctly dark olive green compared to older strata (>10 mbsf) that are black or grey. Second, beds commonly preserve bioturbation in upper bed intervals (Fig. 3), suggesting that the basin floor was bathed in oxygenated, food-rich waters that promoted recolonization after the emplacement of turbidites, and resumption of hemipelagic deposition during MIS1 (Howarth et al. 2021). Similar characteristics have been described from MIS1-aged sediment cores to the north (Fig. 2A; core MD3008, Pouderoux et al. 2012a) and east (Fig. 1; cores Q858-861, Fenner et al. 1992) of Site U1520, as well as across the eastern margin of the South Island, attributed to changes in productivity and terrigenous sediment input (Griggs et al. 1983).

Previous work has suggested that extensive contourite drifts along the upper Hikurangi margin were developed under the ECC, and that channel-overbank sediment waves in the Hikurangi Trough were modified by the East Cape and Deep Western Boundary currents (Bailey et al. 2021). However, more recent detailed quantitative geomorphological and seismic reflection studies of the proximal axial Hikurangi Channel by Tek et al. (2021a, b) do not support the latter interpretation. The average near bottom velocities modelled at Site U1520 (0.06 ms^{-1}) appear insufficient to erode the silt dominated sediments observed (e.g., Postma, 1967), though further analysis is required to determine if mean flow-speeds could sustain transportation of suspended silt-clay introduced via gravity-flows within the near-bottom nepheloid layer. The maximum modelled near-bottom flow velocities (0.35 ms^{-1}) however, are more significant and likely exceed the threshold for fine sediment erosion and entrainment (Figs. S8 and S9; Hollister and McCave, 1984; McCave and Hall, 2006). Thus, despite the absence of a moat and/or sediment drift architecture at Site U1520 (Fig. 2B), discrete erosional events, bottom current reworking, and deposition of mixed and combined turbidite-contourite beds (*sensu* Miramontes et al. 2020. 2021) cannot be ruled out.

Our age model reveals an interesting SAR distribution through the 59 stacked gravity flow beds of MIS1 (Fig. 4). Despite the mean rate of 0.86 m/kyr, SARs down-core begin with an initial peak of 1.28 m/kyr at ~2.4 ka, decreasing to ~0.3 m/kyr at ~3.4 ka, and followed by a steady increase which plateaus at ~1 m/kyr from 11.2-14.5 ka (Fig. 4). Similarly-aged SAR peaks are observed within proximal cores from nearby lower slope basins (MD06-3002, MD06-3003, and MD06-3009), though not on the basin floor to the north (MD06-3008) (Figs. 7 and S7) (Pouderoux et al. 2012a). This suggests that sediment flux to the margin was highly variable through MIS1, possibly driven by changes in sediment supply, sediment source and routing direction (e.g., Kuehl et al. 2016; Bostock et al. 2019a, b), or gravity flow triggering frequencies along different sections of the subduction zone. This is supported by the bed recurrence interval (RI), which is highly variable through MIS1 with a minimum of 143 years (2-3 ka), maximum of ~1000 years (4-5 ka), and mean value of ~322 yrs (Fig. 5). These values are in general agreement with the range of reported mid and late Holocene RIs across the margin (e.g., MD3003, ~270 yrs, Pouderoux et al. 2012b; ~140 yrs Kaikōura Canyon, Mountjoy et al. 2018).

Planktonic foraminiferal assemblages (Table S4) show high oceanicity and regional SSTs steadily increasing up-section from 14.5-11.7 ka (10-6.5 mbsf), likely representing the increased influence of the Tasman Front resulting in a greater inflow of warm ECC from the north (Bostock et al. 2006), and reduced flow of cool Subantarctic Water (SAW) in the Wairarapa Coastal Current (WCC) from the south (Carter et al. 2008). Sea level rise would have also allowed greater flow of STW through Cook Strait, influencing the WCC (Carter et al. 2008) and potentially increasing sediment influx through Cook Strait.

Furthermore, this eustatic change had a profound effect on sediment transport and deposition across the northern Hikurangi margin, in particular by shifting primary depocenters from the slope to the shelf (Lewis 1973, Foster and Carter, 1997; Barnes et al. 2002; Carter et al. 2002; Orpin, 2004; Paquet et al. 2009; 2011; Gerber et al. 2010) and reducing regional along-shore sediment delivery to canyon heads (Fig. 2; e.g., Herzer, 1981; Mountjoy et al 2009; Pouderoux et al. 2012a, b).

Marine Isotope Stage 2:

Sand-silt gravity flow deposits dominate MIS2, with a total of 437 beds identified through this interval. The upper core section between 10-56 mbsf (14.5-24 ka) has beds 0.01-1.7 m thick (Fig. 5). These relatively dark-coloured bi-partite beds likely formed primarily via mud-rich gravity flows (Piper, 1978; Stow and Shanmugam, 1980; Stow and Piper, 1984; Talling et al. 2012; Strachan et al. 2016). In contrast, the lower section spanning 56-95 mbsf (~24-29 ka) is dominated by sandier beds of up 6.39 m in thickness that resulted in reduced core recovery during drilling (Fig. 4; Barnes et al. 2019). These beds display characteristics, such as massive and laminated sands, that are consistent with bedforms expected to be formed via incremental deposition within higher-density turbidity currents and *en masse* deposition of debris flow portions of transitional flows (see SI; Baas et al. 2009; Haughton et al. 2009; Talling et al. 2012; Postma and Cartigny, 2014).

Planktonic foraminiferal assemblages are highly variable, with reduced oceanicity due to the presence of shelfal faunas (Figs. 4 and 6). From 14.5-24 ka (10-56 mbsf) benthic foraminifera indicate sediment sources from shelf environments (0-200 mbsl), whereas down-core, from ~24-29 ka (56-95 mbsf), they were sourced from depths ranging from 0-1000 mbsl (Fig. 4). Throughout this time (14.5-29 ka) there was also a marked increase in Miocene/Pliocene planktonic species in gravity flow deposits (Fig. 6; Crundwell and Woodhouse, Submitted), interpreted to have resulted from enhanced fluvial and coastal erosion of terrestrial outcrops, and submarine erosion of canyon flanks and structural ridges driven by low glacio-eustatic sea level (Barnes et al. 2002, 2018; Paquet et al. 2009; Mountjoy and Barnes, 2011).

The SARs at Site U1520 increase abruptly down-core from the base of MIS1 into MIS2 (Fig. 4). The SAR is 5-6 m/kyr between 14.5-20 ka (~10-33 mbsf), increasing abruptly to 8-10 m/kyr between ~20-22 ka (33-49 mbsf). The staggering maximum rate of ~10 m/kyr occurs at ~21 ka (41 mbsf) during the peak of the LGM (Fig. 4; Barrell et al. 2013; Lambeck et al. 2014; Williams et al. 2015). The SAR reduces to 3.5 m/kyr between 22-24 ka (49-57 mbsf) and returns to very high values of 8-9 m/kyr through the sandy interval between 24-29 ka (57-95 mbsf). These data reveal that peak LGM sedimentation rates were an order of magnitude greater than those documented during MIS1 (Figs. 4 and 7, SI), prior to anthropogenic landscape alterations (McGlone et al. 1994; McGlone and Wilmshurst, 1999; Paquet et al. 2009; Pouderoux et al. 2012a; Kuehl et al. 2016).

A six-fold decrease in mean bed RI occurs down-core from MIS1 (~322 yrs) to MIS2 (~49 yrs). The median RI varies with age in MIS2, decreasing from about 90 yrs at 14.5 ka (~10 mbsf) to its minima of ~14 yrs at the peak of the LGM (~21 ka) (Fig. 5). Peaks of increased median RI are notable at ~18 and 26 ka, the latter of which coincides with the maximum achieved bed thickness through MIS2.

The very short RIs between gravity flows during MIS2 may explain the relative absence of hemipelagic sediment accumulation between gravity flow deposits. However, these SARs and RIs do not account for the lack of bioturbation prior to MIS1, recorded ~8 months after the emplacement of modern turbidites (Howarth et al. 2021). More likely explanations for the lack of bioturbation during MIS2 include insufficient organic carbon content within sandy sediments, a change in the oxygen levels at the seafloor caused by an alteration in the LCDW/DWBC (Hall et al. 2001; McCave et al. 2008), an increase in the dominance of the oxygen deficient Pacific Deep Water (McCave et al. 2008); or a substantial switch in the nature of seafloor environments triggered by the distinct sedimentary processes associated with MIS2.

The significant changes in SAR and bed RI appear to have been strongly influenced by changes in climatic and eustatic conditions. Fluvial systems of both the

North and South islands aggraded significantly during MIS2 (e.g., Litchfield, 2003; Litchfield and Berryman, 2005, 2006; Alloway et al. 2007). In the North Island, cooler, drier conditions, reduced vegetation cover, and increased catchment erosion (McGlone et al. 1993; McGlone, 2001; Turney et al. 2003; Gomez et al. 2004; Paquet et al. 2009; Newnham et al. 2013; Upton et al. 2013) likely doubled the present-day terrigenous load of east coast rivers (Gomez et al. 2004; Paquet et al. 2009; Upton et al. 2013; Kuehl et al. 2016), whilst an intensified glacial circumpolar wind system caused greater aeolian deposition (Stewart and Neall, 1984). With LGM sea level ~120 m below present day (e.g., Gibb, 1986; Pillans et al. 1998; Spratt and Lisiecki, 2016), direct tapping of nearshore sediment transport systems by shelf-indenting gullies and canyon heads promoted increased sediment supply to the Hikurangi Trough (Fig. 2A; Herzer 1981; Lewis and Barnes, 1999; Orpin 2004; Mountjoy et al. 2009, 2013; Pouderoux et al. 2012a, b; McArthur and McCaffrey, 2019; Fisher et al. 2021). Major canyons on the southern HSM increased sediment volumes to the Hikurangi Channel (e.g., Herzer 1981), while northern Hikurangi rivers supplied increased sediment to the trough floor via Māhia Canyon and the Ruatoria re-entrant (e.g., Orpin 2004; Lewis et al. 2004; Carter et al. 2010; Culver et al. 2012; Pouderoux et al. 2012a, b; Upton et al. 2013; Kuehl et al. 2016). Additionally, major Hawke Bay rivers drained to the LGM shoreline on the edge of the shelf, where waves and currents moved sediment alongshore to be redistributed to slope basins (Fig. 2) (Paquet et al. 2009; Hopkins et al. 2020). The LGM WCC was likely intensified by stronger northeastward inflow of SAW and may have contributed to increased northeastward transport of suspended sediment on the upper slope (Foster and Carter, 1997; Nelson et al. 2000b; Chiswell, 2000; Carter et al. 2002; Orpin, 2004; Carter and Manighetti, 2006), however further detailed provenance work is required.

A comparison of sea-level (Spratt and Lisiecki, 2016) with the SAR at Site U1520 suggests that the abrupt increase in median SAR at the base of MIS2 coincides with a sea-level fall from -80 m to -120 m (Fig. 8). We suggest that the initiation of MIS2, and onset of thick sandy beds at Site U1520, marks a critical sea-level threshold at -110±10 m. At this sea level the upper reaches of Māhia Canyon and numerous others along the length of the margin (Figs. 1 and 2) became strongly connected to the shelf sediment supply, were rapidly fluxed with sediment, and changed from silty to sandy staging areas (Figs 2A, 4 and 8). Furthermore, large storm waves and major fluvial flood events could have triggered turbidity currents in addition to earthquakes (McGlone et al. 1993; Mulder et al. 2003; Turney et al. 2003; Gomez et al. 2004; Alloway et al. 2007; Paquet et al. 2009; Carter et al. 2010; Newnham et al. 2013; Paull et al. 2014; Kuehl et al. 2016). Moreover, whereas the MIS1 average turbidite frequency at Site U1520 is close to the regional paleoearthquake recurrence (Pouderoux et al. 2012a, b), the shorter turbidite RI through MIS2 (<50 yrs) is suggestive of additional triggers of turbidity currents, assuming no change in paleoearthquake occurrence.

Interestingly, the thickest sandy beds at Site U1520 were emplaced between 24-29 ka (57-95 mbsf), relatively early in MIS2, and prior to the peak LGM (~21 ka, ~41 mbsf), when global sea levels were lowest. This discrepancy may indicate that: (1) the hypothesized sea level threshold is active in the interval leading up to the lowstand, but not during the LGM itself, (2) the activated sandy staging areas were totally depleted between the initiation of MIS2 (~29 ka, ~95 mbsf) and the peak LGM (~21 ka, ~41 mbsf), or (3) the depocenter for thick sandy beds at Site U1520 migrated elsewhere after 24 ka (Shorrock, 2021).

Marine Isotope Stage 3:

The 109 MIS3 beds are similar to those documented during the upper section (10-56 mbsf) of MIS2, measuring 0.01-0.9 m thick with dark-coloured lower sections, and formed via gravity flows. The MIS2/3 boundary is evident from a marked up-core increase in $\delta^{18}O_{Planktonic}$ at ~29 ka (~95 mbsf; Fig. 4). Planktonic foraminifera show that ocean temperatures were cool during late MIS3, similar to MIS2, likely with a strong influence of SAW coming through the Mernoo Gap at the western end of Chatham Rise (Nelson et al. 2000b) (Fig. 1). The lithology and benthic foraminiferal paleo-water depth signal present within MIS3 share affinity with those within the upper MIS2 sediments (~10-56 mbsf; Fig. 4); contrastingly however, there are little to no reworked Miocene/Pliocene foraminifera (Fig. 6).

The MIS2/3 transition at Site U1520 marks a dramatic down-core reduction in SARs to a mean value of 0.78 m/kyr in MIS3 (Figs. 4 and 7), comparable with MIS1 (mean 0.86 m/kyr). The bed RI ranges from ~100-200 yrs between 30-40 ka, increasing to 1000 yrs prior to 40 ka (Fig. 5). The mean bed RI increases to ~231 yrs (cf. 322 yrs in MIS1 and 49 yrs in MIS2). Figures 5 and 8 illustrate that sea level in MIS3 ranged from about -80 m below present at 40 ka to about -110 m below present at the MIS2/3 transition. These sea levels during MIS3 appear to have been favourable for silty sediment supply to the Hikurangi Trough floor.

Global Context and Implications of SARs in Subduction Margins

We compiled SAR data at core sites from global subduction trenches for comparison with Site U1520 in the northern Hikurangi Trough (Fig. S10 and Table S6). Numerous gravity core studies over timeframes of <17 ka report mean SARs of <2 m/kyr, which show a decrease in rates to <0.2 m/kyr into the Holocene (e.g., Nelson, 1976; Stanley et al. 1978; Blumberg et al. 2008; Ratzov et al. 2010; Goldfinger et al. 2012, 2017; Pouderoux et al. 2012a, b; Polonia et al. 2013; Paull et al. 2014; Patton et al. 2015; Ikehara et al. 2016; Hsiung et al. 2021). Notably however, Bourget et al. (2010) reported little change in the bulk SAR off Makran where rates of mainly clastic and minor carbonate sedimentation have remained between 1.0-1.7 m/kyr from 0-35 ka. However, very few studies have presented high-resolution (10^3-10^4 yrs) assessments of SARs spanning MIS1-3 with notable exceptions from Knudson and Hendy (2009) who demonstrated a 6-fold increase in SAR on the distal Nitinat Fan, Cascadia (~0.3 m/kyr <10 ka to 1.9 m/kyr 16-74 ka), and Blumberg et al. (2008) who suggested a 15-fold increase in SAR (~0.1 m/kyr <18 ka to 1.5 m/kyr 18-35 ka) from the Chilean Trench. These studies demonstrate that despite regional and site-specific differences in absolute SARs, the order of magnitude increase in SAR during the LGM at Site U1520 is not unique.

SARs documented at core sites in trenches comparable to the ~10 m/kyr MIS2 rate determined at northern Hikurangi IODP Site U1520 (Table S6) are unusual. It appears that specific environmental factors are required to deliver this high volume of sediment to the trench (e.g., Bernhardt et al. 2017; McArthur and Tek, 2021). Zuffa et al. (2000) reported exceptional SARs of up to 15 m/kyr between 19-35 ka on the outer Astoria Fan off Cascadia. These rates result from the emplacement of extremely thick (up to 60 m) beds on the incoming plate due to Jökulhlaups (glacial outbursts) of glacial lakes in the western United States. SARs of up to 16 m/kyr during the interval 8-13 ka on the Eel Fan off southern Cascadia were reported by Paull et al. (2014). They demonstrated that: (1) these rates reflect the former direct connection of the Eel River with the Eel Canyon head, enhancing the role of the canyon as an efficient source to sink conduit, and (2) the sub-decadal (7 yrs) average turbidite frequency indicates triggers other than earthquakes, likely including river flood-discharge hyperpycnal flows.

In contrast, the long-term average SARs at northern Hikurangi Site U1520 (2.4 m/kyr over 45 ka, this study; ~0.7 m/kyr over ~500 ka, and ~0.5 m/kyr over ~780 ka, Barnes et al. 2019) (Table S6) appear to be comparable to several other trenches (Fig. S10) (e.g., von Huene and Kulm, 1973; Westbrook et al. 1994; Harris et al. 2013; Hsiung et al. 2015; McNeill et al. 2017; Underwood and Pickering, 2018; Pickering et al. 2020). Collectively, these data indicate that: (1) SARs over long-term timeframes of 10^5-10^6 years do not capture high variability of climatic-eustatic cyclicity at 10^3-10^4 years, (2) maximum SARs of ~ 10 m/kyr in MIS2 recorded at Site U1520 are very high, and (3) recent SARs at Site U1520 over 45 ka exceed longer term averages over ~800 ka (Crundwell and Woodhouse, Submitted; Noda et al. Submitted).

Conclusions

Dating and age modelling reveals the upper 110 m of siliciclastic sediments in the northern Hikurangi Trough at IODP Site U1520 spans the entirety of MIS1, 2, and the latter part of MIS3 (0-45 ka). The sedimentary succession is dominated by stacked sand-silt gravity flow deposits up to ~6.4 m thick, comprising abundant reworked material, interspersed with minor macroscopic volcanic tephra. The mean bed RI varies from ~322 yrs in MIS1, ~49 yrs in MIS2, and ~231 yrs in MIS3. Large (6-fold) and abrupt variations in SAR are recorded across MIS transitions, with peak rates of ~10 m/kyr during the LGM, and <1m/kyr during MIS1 and 3.

We infer that the very high glacial SARs at northern Hikurangi Site U1520 resulted primarily from a combination of (1) increased erosion in some terrestrial catchments and associated increase in fluvial sediment supply, (2) a critical lowering of eustatic sea level that was accompanied by increased charging of submarine canyons and gully systems (including the local Māhia Canyon and regional Cook Strait, Kaikōura and Pegasus canyons feeding the southern Hikurangi Channel), and (3) increased frequency of margin-bypassing (e.g., Stevenson et al. 2015) turbidity currents as suggested by minimum RI values. The balance among different point sources and routing directions may have changed over time, but the Hikurangi Trough floor is a good example of a sustained system (Covault and Graham, 2010), characterized by frequent gravity-flow events occurring during both highstand and lowstand conditions.

A global comparison of trench settings indicates that the northern Hikurangi LGM SARs at IODP Site U1520 are equivalent to the highest recorded linear rates from core sites in other trenches, and that average SARs determined over long-term timeframes of 10^5-10^6 years may not capture potential high variability at climatic-eustatic cyclicity over 10^3-10^4 years.

Data Availability Statement

The supplementary information, ten supplementary figures, and six supplementary tables that support the findings of this study are openly available in figshare at https://doi.org/10.6084/m9.figshare.19391531.v2.

Acknowledgements

This research used samples and data provided by the International Ocean Discovery Program (IODP). Funding for this research was provided through UKIODP by the Natural Environmental Research Council (NERC Grant NE/S008853/1), the New Zealand Ministry for Business Innovation and Employment (MBIE) Contract CO5X1605, NIWA Science Core funding Programme COPR, and the New Zealand Marsden Fund Contract 20-UOA-099. K. Pank and S. Kutterolf have been supported by the German Research foundation, DFG, within the project KU2685/11-1. L. LeVay and K. Petronotis were supported by IODP-JRSO NSF Award 1326927. We would also like to extend our thanks to Michael Underwood and Atsushi Noda for useful discussion on the manuscript, Alan Orpin for assistance with radiocarbon calibrations, and Francisco

Saldana-Monroy for interpretation of bioturbation structures. We thank Lionel Carter, Fabien Paquet, and two anonymous reviewers for constructive and insightful reviews of the manuscript.

References

Alloway, B.V., Lowe, D.J., Barrell, D.J., Newnham, R.M., Almond, P.C., Augustinus, P.C., Bertler, N.A., Carter, L., Litchfield, N.J., McGlone, M.S., Shulmeister, J., 2007. Towards a climate event stratigraphy for New Zealand over the past 30 000 years (NZ-INTIMATE project). Journal of Quaternary Science, 22(1), 9-35.

Ashley, G.M. 1990. Classification of large-scale subaqueous bedforms: A new look at an old problem. Journal of Sedimentary Petrology, 60, 160–172.

Aubouin, J., von Huene, R., et al. 1982a. Site 499: Middle America Trench axis, in Aubouin, J., von Huene, R., et al., Initial reports of the Deep Sea Drilling Project, Volume 67: Washington, D.C., U.S. Government Printing Office, 267-314.

Aubouin, J., von Huene, R., et al. 1982b. Site 500: Middle America Trench axis, in Aubouin, J., von Huene, R., et al., Initial reports of the Deep Sea Drilling Project, Volume 67: Washington, D.C., U.S. Government Printing Office, 267-314.

Baas, J.H., Best, J.L., Peakall, J. and Wang, M., 2009. A phase diagram for turbulent, transitional, and laminar clay suspension flows. Journal of Sedimentary Research, 79(4), 162-183.

Baas, J.H., Best, J.L., Peakall, J. 2011. Depositional processes, bedform development and hybrid bed formation in rapidly decelerated cohesive (mud–sand) sediment flows. Sedimentology, 58(7), 1953-1987.

Baas, J.H., Best, J.L., Peakall, J. 2016. Predicting bedforms and primary current stratification in cohesive mixtures of mud and sand. Journal of the Geological Society, 173(1), 12-45.

Backman, J., Chen, W., Kachovich, S., Mitchison, F., Petronotis, K., Yang, T., Zhao, X. 2019. Data report: revised age models for IODP Sites U1480 and U1481, Expedition 362. Proceedings of the International Ocean Discovery Program, 362.

Bailey, W.S., McArthur, A.D., McCaffrey, W.D. 2020. Distribution of contourite drifts on convergent margins: Examples from the Hikurangi subduction margin of New Zealand. Sedimentology.

Bailey, W., McArthur, A., McCaffrey, W. 2021. Sealing potential of contourite drifts in deep-water fold and thrust belts: Examples from the Hikurangi Margin, New Zealand. Marine and Petroleum Geology, 123, 104776.

Baldwin, B., Butler, C.O. 1985. Compaction curves. AAPG bulletin, 69(4), 622-626.

Barker, D.H., Henrys, S., Caratori Tontini, F., Barnes, P.M., Bassett, D., Todd, E. Wallace, L. 2018. Geophysical constraints on the relationship between seamount subduction, slow slip, and tremor at the north Hikurangi subduction zone, New Zealand. Geophysical Research Letters, 45(23), 12-804.

Barnes, P.M., Nicol, A., Harrison, T. 2002. Late Cenozoic evolution and earthquake potential of an active listric thrust complex above the Hikurangi subduction zone, New Zealand. GSA Bulletin, 114(11), 1379-1405.

Barnes, P.M., Lamarche, G., Bialas, J., Henrys, S., Pecher, I., Netzeband, G.L., Greinert, J., Mountjoy, J.J., Pedley, K., Crutchley, G. 2010. Tectonic and geological framework for gas hydrates and cold seeps on the Hikurangi subduction margin, New Zealand. Marine Geology, 272(1-4), 26-48.

Barnes, P.M., Ghisetti, F.C., Ellis, S., Morgan, J.K. 2018. The role of protothrusts in frontal accretion and accommodation of plate convergence, Hikurangi subduction margin, New Zealand. Geosphere, 14(2), 440-468.

Barnes, P.M., Wallace, L.M., Saffer, D.M., Pecher, I.A., Petronotis, K.E., LeVay, L.J., Bell, R.E., Crundwell, M.P., Engelmann de Oliveira, C.H., Fagereng, A., Fulton, P.M., Greve, A., Harris, R.N., Hashimoto, Y., Hüpers, A., Ikari, M.J., Ito, Y., Kitajima, H., Kutterolf, S., Lee, H., Li, X., Luo, M., Malie, P.R., Meneghini, F., Morgan, J.K., Noda, A., Rabinowitz, H.S., Savage, H.M., Shepherd, C.L., Shreedharan, S., Solomon, E.A., Underwood, M.B., Wang, M., Woodhouse, A.D., Bourlange, S.M., Brunet, M.M.Y., Cardona, S., Clennell, M.B., Cook, A.E., Dugan, B., Elger, J., Gamboa, D., Georgiopoulou, A., Han, S., Heeschen, K.U., Hu, G., Kim, G.Y., Koge, H., Machado, K.S., McNamara, D.D., Moore, G.F., Mountjoy, J.J., Nole, M.A., Owari, S., Paganoni, M., Rose, P.S., Screaton, E.J., Shankar, U., Torres, M.E., Wang, X., Wu, H.-Y. 2019. Site U1520. In Wallace, L.M., Saffer, D.M., Barnes, P.M., Pecher, I.A., Petronotis, K.E., LeVay, L.J., and the Expedition 372/375 Scientists, Hikurangi Subduction Margin Coring, Logging,and Observatories. Proceedings of the International Ocean Discovery Program, 372B/375: College Station, TX (International OceanDiscovery Program).

Barnes, P.M., Wallace, L.M., Saffer, D.M., Bell, R.E., Underwood, M.B., Fagereng, A., Meneghini, F., Savage, H.M., Rabinowitz, H.S., Morgan, J.K., Kitajima, H. et al. 2020. Slow slip source characterized by lithological and geometric heterogeneity. Science Advances, 6(13), p.eaay3314.

Barrell, D.J.A. 2013. Late Quaternary of the Southwest Pacific Region. In: Elias S.A. (ed.) The Encyclopedia of Quaternary Science, vol. 2, 202-215. Amsterdam: Elsevier.

Barrell, D.J., Almond, P.C., Vandergoes, M.J., Lowe, D.J., Newnham, R.M., INTIMATE members. 2013. A composite pollen-based stratotype for inter-regional evaluation of climatic events in New Zealand over the past 30,000 years (NZ-INTIMATE project). Quaternary Science Reviews, 74, 4-20.

Behrens, E., Hogg, A. M., England, M. H., Bostock, H. 2021. Seasonal and interannual variability of the Subtropical Front in the New Zealand region. Journal of Geophysical Research: Oceans, 126, e2020JC016412. https://doi.org/10.1029/2020JC016412.

Bell, R., Sutherland, R., Barker, D.H., Henrys, S., Bannister, S., Wallace, L., Beavan, J. 2010. Seismic reflection character of the Hikurangi subduction interface, New Zealand, in the region of repeated Gisborne slow slip events. Geophysical Journal International, 180(1), 34-48.

Bernhardt, A., Schwanghart, W., Hebbeln, D., Stuut, J.B.W., Strecker, M.R. 2017. Immediate propagation of deglacial environmental change to deep-marine turbidite systems along the Chile convergent margin. Earth and Planetary Science Letters, 473, 190-204.

Berryman, K., Marden, M., Eden, D., Mazengarb, C., Ota, Y., Moriya, I. 2000. Tectonic and paleoclimatic significance of Quaternary river terraces of the Waipaoa River, east coast, North Island, New Zealand. New Zealand Journal of Geology and Geophysics 43, 229–245.

Blumberg, S., Lamy, F., Arz, H.W., Echtler, H.P., Wiedicke, M., Haug, G.H., Oncken, O. 2008. Turbiditic trench deposits at the South-Chilean active margin: a Pleistocene–Holocene record of climate and tectonics. Earth and Planetary Science Letters, 268(3-4), 526-539.

Bostock, H.C., Opdyke, B.N., Gagan, M.K., Kiss, A.E., Fifield, L.K. 2006. Glacial/interglacial changes in the East Australian current. Climate Dynamics, 26(6), 645-659.

Bostock, H., Jenkins, C., Mackay, K., Carter, L., Nodder, S., Orpin, A., Pallentin, A., Wysoczanski, R. 2019a. Distribution of surficial sediments in the ocean around New Zealand/Aotearoa. Part A: continental slope and deep ocean. New Zealand Journal of Geology and Geophysics, 62(1), 1-23.

Bostock, H., Jenkins, C., Mackay, K., Carter, L., Nodder, S., Orpin, A., Pallentin, A., Wysoczanski, R. 2019b. Distribution of surficial sediments in the ocean around New Zealand/Aotearoa. Part B: continental shelf. New Zealand Journal of Geology and Geophysics, 62(1), 24-45.

Bourget, J., Zaragosi, S., Ellouz-Zimmermann, S., Ducassou, E., Prins, M.A., Garlan, T., Lanfumey, V., Schneider, J.L., Rouillard, P., Giraudeau, J. 2010. Highstand vs. lowstand turbidite system growth in the Makran active margin: Imprints of high-frequency external controls on sediment delivery mechanisms to deep water systems. Marine Geology, 274(1-4), 187-208.

Bourget, J., Zaragosi, S., Ellouz-Zimmermann, N., Mouchot, N., Garlan, T., Schneider, J.-L., Lanfumey, V., Lallemant, S. 2011, Turbidite system architecture and sedimentary processes along topographically complex slopes: The Makran convergent margin: Sedimentology, 58, 376–406, https://doi.org/10.1111/j.1365-3091.2010.01168.x.

Brodie, J.W.I. 1960. Coastal surface currents around New Zealand. New Zealand Journal of Geology and Geophysics, 3: 235–252.

Caley, T., Malaizé, B., Zaragosi, S., Rossignol, L., Bourget, J., Eynaud, F., Martinez, P., Giraudeau, J., Charlier, K., Ellouz-Zimmermann, N. 2011. New Arabian Sea records help decipher orbital timing of Indo-Asian monsoon. Earth and Planetary Science Letters, 308(3-4), 433-444.

Campbell, K.A., Nelson, C.S., Alfaro, A.C., Boyd, S., Greinert, J., Nyman, S., Grosjean, E., Logan, G.A., Gregory, M.R., Cooke, S., Linke, P. 2010. Geological imprint of methane seepage on the seabed and biota of the convergent Hikurangi Margin, New Zealand: Box core and grab carbonate results. Marine Geology, 272(1-4), 285-306.

Carter, L., Manighetti, B. 2006. Glacial/interglacial control of terrigenous and biogenic fluxes in the deep ocean off a high input, collisional margin: A 139 kyr-record from New Zealand. Marine geology, 226(3-4), 307-322.

Carter, L., McCave, I.N. 1994. Development of sediment drifts approaching an active plate margin under the SW Pacific Deep Western Boundary Current. Paleoceanography 9, 1061–1085. https://doi.org/10.1029/94PA01444.

Carter, L., Nelson, C.S., Neil, H.L. Froggatt, P.C. 1995. Correlation, dispersal, and preservation of the Kawakawa Tephra and other late Quaternary tephra layers in the Southwest Pacific Ocean. New Zealand Journal of Geology and Geophysics, 38(1), 29-46.

Carter, L., Manighetti, B., Elliot, M., Trustrum, N., Gomez, B. 2002. Source, sea level and circulation effects on the sediment flux to the deep ocean over the past 15 ka off eastern New Zealand. Global and Planetary Change, 33, 339-355.

Carter, L., Manighetti, B., Ganssen, G., Northcote, L. 2008. Southwest Pacific modulation of abrupt climate change during the Antarctic Cold Reversal–Younger Dryas. Palaeogeography, Palaeoclimatology, Palaeoecology, 260(1-2), 284-298.

Carter, L., Orpin, A.R., Kuehl, S.A. 2010. From mountain source to ocean sink–the passage of sediment across an active margin, Waipaoa Sedimentary System, New Zealand. Marine Geology, 270(1-4), 1-10.

Chiswell, S.M. 2000. The Wairarapa coastal current. New Zealand Journal of Marine and

Freshwater Research, 34(2), 303-315.

Chiswell, S.M. 2005. Mean and variability in the Wairarapa and Hikurangi eddies, New Zealand. New Zealand Journal of Marine and Freshwater Research, 39(1), 121-134.

Chiswell, S.M., Bostock, H.C., Sutton, P.J., Williams, M.J. 2015. Physical oceanography of the deep seas around New Zealand: a review. New Zealand Journal of Marine and Freshwater Research, 49(2), 286-317.

Cita, M.B., Broglia, C., Malinverno, A., Spezzibottiani, G., Tomadin, L., Violanti, D. 1982. Late Quaternary pelagic sedimentation on the southern Calabrian Ridge and western Mediterranean Ridge, eastern Mediterranean. Marine Micropaleontology, 7(2), 135-162.

Clark, P.U., Dyke, A.S., Shakun, J.D., Carlson, A.E., Clark, J., Wohlfarth, B., Mitrovica, J.X., Hostetler, S.W., McCabe, A.M. 2009. The last glacial maximum. Science, 325(5941), 710-714.

Clark, K., Howarth, J., Litchfield, N., Cochran, U., Turnbull, J., Dowling, L., Howell, A., Berryman, K., Wolfe, F. 2019. Geological evidence for past large earthquakes and tsunamis along the Hikurangi subduction margin, New Zealand. Marine Geology, 412, 139-172.

Claussmann, B., Bailleul, J., Chanier, F., Caron, V., McArthur, A.D., Mahieux, G., Chaptal, C., Vendeville, B.C. 2021. Contrasting mixed siliciclastic-carbonate shelf-derived gravity-driven systems in compressional intra-slope basins (southern Hikurangi margin, New Zealand). Marine and Petroleum Geology, 134, 105252.

Claussmann, B., Bailleul, J., Chanier, F., Mahieux, G., Caron, V., McArthur, A.D., Chaptal, C., Morgans, H.E., Vendeville, B.C. 2022. Shelf-derived mass-transport deposits: origin and significance in the stratigraphic development of trench-slope basins. New Zealand Journal of Geology and Geophysics, 65(1), 17-52.

Collot, J.Y., Delteil, J., Lewis, K.B., Davy, B., Lamarche, G., Audru, J.C., Barnes, P., Chanier, F., Chaumillon, E., Lallemand, S., de Lepinay, B.M. 1996. From oblique subduction to intra-continental transpression: Structures of the southern Kermadec-Hikurangi margin from multibeam bathymetry, side-scan sonar and seismic reflection. Marine Geophysical Researches, 18(2), 357-381.

Collot, J.Y., Lewis, K., Lamarche, G., Lallemand, S. 2001. The giant Ruatoria debris avalanche on the northern Hikurangi margin, New Zealand: Result of oblique seamount subduction. Journal of Geophysical Research: Solid Earth, 106(B9), 19271-19297.

Covault, J.A., Graham, S.A. 2010. Submarine fans at all sea-level stands: Tectono-morphologic and climatic controls on terrigenous sediment delivery to the deep sea. Geology, 38(10), 939-942.

Covault, J.A., Shelef, E., Traer, M., Hubbard, S.M., Romans, B.W., Fildani, A. 2012. Deep-water channel run-out length: Insights from seafloor geomorphology. Journal of Sedimentary Research, 82(1), 21-36.

Crundwell, M.P., Woodhouse, A. 2022. A detailed biostratigraphic framework for 0–1.2 Ma Quaternary sediments of north-eastern Zealandia. New Zealand Journal of Geology and Geophysics, 1-14.

Crundwell, M.P., Woodhouse, A. (Submitted). Biostratigraphically constrained chronologies for Quaternary sequences from the Hikurangi margin of north-eastern Zealandia. New Zealand Journal of Geology and Geophysics.

Crundwell, M.P., Scott, G.H., Thrasher, G.P. 1994. Calibration of paleobathymetry indicators by integrated seismic and paleontological analysis of foreset sequences, Taranaki Basin, New Zealand. In 1994 New Zealand Petroleum Conference Proceedings, 169-178.

Crundwell, M.P., Scott, G., Naish, T., Carter, L. 2008. Glacial–interglacial ocean climate variability from planktonic foraminifera during the Mid-Pleistocene transition in the temperate Southwest Pacific, ODP Site 1123. Palaeogeography, Palaeoclimatology, Palaeoecology, 260(1-2), 202-229.

Culver, S.J., Camp, R.L., Walsh, J.P., Hayward, B.W., Corbett, D.R., Alexander, C.R. 2012. Distribution of foraminifera of the Poverty continental margin, New

Zealand: implications for sediment transport. The Journal of Foraminiferal Research, 42(4), 305-326.

Donoghue, S.L., Neall, V.E. 1996. Tephrostratigraphic studies at Tongariro volcanic centre, New Zealand: an overview. Quaternary International, 34, 13-20.

Eden, D.N., Palmer, A.S., Cronin, S.J., Marden, M., Berryman, K.R. 2001. Dating the culmination of river aggradation at the end of the last glaciation using distal tephra compositions, eastern North Island, New Zealand. Geomorphology 38, 133–151.

Edgar, K.M., Anagnostou, E., Pearson, P.N., Foster, G.L., 2015. Assessing the impact of diagenesis on δ11B, δ13C, δ18O, Sr/Ca and B/Ca values in fossil planktic foraminiferal calcite. Geochimica et Cosmochimica Acta, 166, 189-209.

Ehrmann, W., Schmiedl, G., Beuscher, S., Krüger, S. 2017. Intensity of African humid periods estimated from Saharan dust fluxes. PloS one, 12(1), p.e0170989.

Fenner, J., Carter, L., Stewart, R. 1992. Late Quaternary paleoclimatic and paleoceanographic change over northern Chatham Rise, New Zealand. Marine Geology, 108(3-4), 383-404.

Fisher, D.M., Hooker, J.N., Smye, A.J., Chen, T.W. 2021. Insights from the geological record of deformation along the subduction interface at depths of seismogenesis. Geosphere, 17(6), 1686-1703.

Foster, G., Carter, L. 1997. Mud sedimentation on the continental shelf at an accretionary margin—Poverty Bay, New Zealand. New Zealand Journal of Geology and Geophysics, 40(2), 157-173.

Gase, A.C., Van Avendonk, H.J., Bangs, N.L., Bassett, D., Henrys, S.A., Barker, D.H., Kodaira, S., Jacobs, K.M., Luckie, T.W., Okaya, D.A., Fujie, G. 2021. Crustal structure of the northern Hikurangi margin, New Zealand: Variable accretion and overthrusting plate strength influenced by rough subduction. Journal of Geophysical Research: Solid Earth, 126(5), p.e2020JB021176.

Gerber, T.P., Pratson, L.F., Kuehl, S., Walsh, J.P., Alexander, C., Palmer, A. 2010. The influence of sea level and tectonics on Late Pleistocene through Holocene sediment storage along the high-sediment supply Waipaoa continental shelf. Marine Geology, 270(1-4), 139-159.

Ghisetti, F.C., Barnes, P.M., Ellis, S., Plaza-Faverola, A., Barker, D.H.N. 2016. The last 2 Myr of accretionary wedge construction in the central Hikurangi margin (North Island, New Zealand): Insights from structural modelling: Geochemistry, Geophysics, Geosystems, 17, 2661–2686, https://doi.org /10 .1002 /2016GC006341.

Gibb, J.G. 1986, A New Zealand regional Holocene eustatic sea-level curve and its application for determination of vertical tectonic movements, in Reilly, W.I., and Harford, B.E., eds., Recent Crustal Movements of the Pacific Region: Royal Society of New Zealand, Bulletin, 24, 377–395.

Goldfinger, C., Nelson, C.H., Morey, A.E., Johnson, J.E., Patton, J.R., Karabanov, E.B., Gutierrez-Pastor, J., Eriksson, A.T., Gracia, E., Dunhill, G., Enkin, R.J. 2012. Turbidite event history—Methods and implications for Holocene paleoseismicity of the Cascadia subduction zone (No. 1661-F). US Geological Survey.

Goldfinger, C., Galer, S., Beeson, J., Hamilton, T., Black, B., Romsos, C., Patton, J., Nelson, C.H., Hausmann, R., Morey, A. 2017. The importance of site selection, sediment supply, and hydrodynamics: A case study of submarine paleoseismology on the northern Cascadia margin, Washington USA. Marine Geology, 384, 4-46.

Gomez, B., Carter, L., Trustrum, N.A., Palmer, A.S., Roberts, A.P. 2004. El Niño–Southern Oscillation signal associated with middle Holocene climate change in intercorrelated terrestrial and marine sediment cores, North Island, New Zealand. Geology, 32(8), 653-656.

Gong, C., Wang, Y., Rebesco, M., Salon, S., Steel, R.J. 2018. How do turbidity flows interact with contour currents in unidirectionally migrating deep-water channels? Geology, 46, 551–554.

Gray, M., Bell, R.E., Morgan, J.V., Henrys, S., Barker, D.H., IODP Expedition 372 and 375 Science Parties. 2019. Imaging the shallow subsurface structure of the North

Hikurangi Subduction Zone, New Zealand, using 2-D full-waveform inversion. Journal of Geophysical Research: Solid Earth, 124(8), 9049-9074.

Griggs, G.B., Carter, L., Kennett, J.P., Carter, R.V. 1983. Late Quaternary marine stratigraphy southeast of New Zealand. Geological Society of America Bulletin, 94(6), 791-797.

Hall, I.R., McCave, I.N., Shackleton, N.J., Weedon, G.P., Harris, S.E. 2001. Intensified deep Pacific inflow and ventilation in Pleistocene glacial times. Nature, 412(6849), 809-812.

Harris, P. T., Whiteway, T. 2011. Global distribution of large submarine canyons: Geomorphic differences between active and passive continental margins. Marine Geology, 285, 69–86. https://doi.org/10.1016/j.margeo.2011.05.008

Harris, R.N., Sakaguchi, A., Petronotis, K., Baxter, A.T., Berg, R., Burkett, A., Charpentier, D., Choi, J., Diz Ferreiro, P., Hamahashi, M., Hashimoto, Y., Heydolph, K., Jovane, L., Kastner, M., Kurz, W., Kutterolf, S.O., Li, Y., Malinverno, A., Martin, K.M., Millan, C., Nascimento, D.B., Saito, S., Sandoval Gutierrez, M.I., Screaton, E.J., Smith-Duque, C.E., Solomon, E.A., Straub, S.M., Tanikawa, W., Torres, M.E., Uchimura, H., Vannucchi, P., Yamamoto, Y., Yan, Q., and Zhao, X., 2013. Input Site U1381. In Harris, R.N., Sakaguchi, A., Petronotis, K., and the Expedition 344 Scientists, Proc. IODP, 344: College Station, TX (Integrated Ocean Drilling Program). doi:10.2204/iodp.proc.344.103.2013. Expedition 334 Scientists, 2013. Site U1381. In Vannucchi, P., Ujiie, K., Stroncik, N., Malinverno, A., and the Expedition 334 Scientists, Proc. IODP, 334: Tokyo (Integrated Ocean Drilling Program Management International, Inc.). doi:10.2204/iodp.proc.334.106.2012

Haughton, P., Davis, C., McCaffrey, W., Barker, S. 2009. Hybrid sediment gravity flow deposits–classification, origin and significance. Marine and Petroleum Geology, 26(10), 1900-1918.

Hayward, B.W. 1999. Recent New Zealand shallow-water benthic foraminifera: taxonomy, ecologic distribution, biogeography, and use in paleoenvironmental assessment. Institute of Geological & Nuclear Sciences Monograph, 21, 264.

Hayward, B.W., Carter, R., Grenfell, H.R., Hayward, J.J. 2001. Depth distribution of Recent deep-sea benthic foraminifera east of New Zealand, and their potential for improving paleobathymetric assessments of Neogene microfaunas. New Zealand Journal of Geology and Geophysics, 44(4), 555-587.

Hayward, B.W., Grenfell, H.R., Sabaa, A.T., Neil, H., Buzas, M.A. 2010. Recent New Zealand Deep-Water Benthic Foraminifera: Taxonomy, Ecologic Distribution, Biogeography, and Use in Paleoenvironmental Assessment. Institute of Geological & Nuclear Sciences monograph no. 26, 2010, 363

Hayward, B.W., Sabaa, A.T., Triggs, C.M. 2019. Using foraminiferal test-size distribution and other methods to recognise Quaternary bathyal turbidites and taphonomically-modified faunas. Marine Micropaleontology, 148, 65-77.

Heath, R.A. 1975. Oceanic circulation off the east coast of New Zealand (Vol. 55). New Zealand Oceanographic Institute.

Heaton, T.J., Köhler, P., Butzin, M., Bard, E., Reimer, R.W., Austin, W.E., Ramsey, C.B., Grootes, P.M., Hughen, K.A., Kromer, B., Reimer, P.J. 2020. Marine20—the marine radiocarbon age calibration curve (0–55,000 cal BP). *Radiocarbon*, *62*(4), 779-820.

Herzer, R.H., 1981. Late Quaternary stratigraphy and sedimentation of the Canterbury continental shelf New Zealand. New Zealand Oceanographic Institute Memoir 89.

Ho, V.L., Dorrell, R.M., Keevil, G.M., Burns, A.D., McCaffrey, W.D. 2018. Pulse propagation in turbidity currents. Sedimentology, 65(2), 620-637.

Hollister, C.D., McCave, I.N. 1984. Sedimentation under deep-sea storms. Nature, 309(5965), 220-225.

Hopkins, J.L., Wysoczanski, R.J., Orpin, A.R., Howarth, J.D., Strachan, L.J., Lunenburg, R., McKeown, M., Ganguly, A., Twort, E., Camp, S. 2020. Deposition and preservation of tephra in marine sediments at the active Hikurangi subduction margin. Quaternary Science Reviews, 247, 106500.

Hopkins, J.L., Bidmead, J.E., Lowe, D.J., Wysoczanski, R.J., Pillans, B.J., Ashworth, L., Rees, A.B., Tuckett, F. 2021a. TephraNZ: a major and trace element reference dataset for prominent Quaternary rhyolitic tephras in New Zealand and implications for correlation. Geochronology Discussions, 1-63.

Hopkins, J.L., Lowe, D.J., Horrocks, J.L. 2021b. Tephrochronology in Aotearoa New Zealand. New Zealand Journal of Geology and Geophysics, 64(2-3), 153-200.

Howarth, J.D., Orpin, A.R., Kaneko, Y., Strachan, L.J., Nodder, S.D., Mountjoy, J.J., Barnes, P.M., Bostock, H.C., Holden, C., Jones, K., Cağatay, M.N. 2021. Calibrating the marine turbidite palaeoseismometer using the 2016 Kaikōura earthquake. Nature Geoscience, 14(3), 161-167.

Hsiung, K.H., Su, C.C., Yu, H.S., Chang, J.H. 2015. Morphology, seismic characteristics and development of the sediment dispersal system along the Taiwan–Luzon convergent margin. Marine Geophysical Research, 36(4), 293-308.

Hsiung, K.H., Kanamatsu, T., Ikehara, K., Usami, K., Horng, C.S., Ohkouchi, N., Ogawa, N.O., Saito, S., Murayama, M. 2021. X-ray fluorescence core scanning, magnetic signatures, and organic geochemistry analyses of Ryukyu Trench sediments: turbidites and hemipelagites. Progress in Earth and Planetary Science, 8(1), 1-17.

Hunt, J.B., Hill, P.G. 2001. Tephrological implications of beam size—sample-size effects in electron microprobe analysis of glass shards. Journal of Quaternary Science: Published for the Quaternary Research Association, 16(2), 105-117.

Ikehara, K., Kanamatsu, T., Nagahashi, Y., Strasser, M., Fink, H., Usami, K., Irino, T., Wefer, G. 2016. Documenting large earthquakes similar to the 2011 Tohoku-oki earthquake from sediments deposited in the Japan Trench over the past 1500 years. Earth and Planetary Science Letters, 445, 48-56.

Iverson, R.M. 2005. Debris-flow mechanics. Debris-flow hazards and related phenomena, 105-134.

Jaeger, J.M., Gulick, S.P.S., LeVay, L.J., Asahi, H., Bahlburg, H., Belanger, C.L., Berbel, G.B.B., Childress, L.B., Cowan, E.A., Drab, L., Forwick, M. 2014. Site U1417. In Proceedings of the IODP.

Kane, I.A., Kneller, B.C., Dykstra, M., Kassem, A., McCaffrey, W.D. 2007. Anatomy of a submarine channel-levee: An example from Upper Cretaceous slope sediments, Rosario Formation, Baja California, Mexico. Marine and Petroleum Geology, 24, 540-563.

Kao, S.J., Dai, M., Selvaraj, K., Zhai, W., Cai, P., Chen, S.N., Yang, J.Y.T., Liu, J.T., Liu, C.C., Syvitski, J.P.M. 2010. Cyclone-driven deep sea injection of freshwater and heat by hyperpycnal flow in the subtropics. Geophysical Research Letters, 37(21).

Kimura, G., Silver, E., Blum, P., Fox, P.J., Baldauf, J., Francis, T.J. 1997. Ocean Drilling Program Leg 170 Scientific Prospectus Costa Rica Accretionary Wedge.

Kiyokawa, S., Yokoyama, K. 2009. Provenance of turbidite sands from IODP EXP 1301 in the northwestern Cascadia Basin, western North America. Marine Geology, 260(1-4), 19-29.

Kneller, B. 1995. Beyond the turbidite paradigm: physical models for deposition of turbidites and their implications for reservoir prediction. Geological Society, London, Special Publications, 94(1), 31-49.

Kneller, B. and Buckee, C. 2000. The structure and fluid mechanics of turbidity currents: a review of some recent studies and their geological implications. Sedimentology, 47, 62-94.

Knudson, K.P., Hendy, I.L. 2009. Climatic influences on sediment deposition and turbidite frequency in the Nitinat Fan, British Columbia: Marine Geology, v. 262, 29-38.

Kuehl, S.A., Alexander, C.R., Blair, N.E., Harris, C.K., Marsaglia, K.M., Ogston, A.S., Orpin, A.R., Roering, J.J., Bever, A.J., Bilderback, E.L., Carter, L. 2016. A source-to-sink perspective of the Waipaoa River margin. Earth-Science Reviews, 153, 301-334.

Lambeck, K., Rouby, H., Purcell, A., Sun, Y., Sambridge, M. 2014. Sea level and global ice volumes from the Last Glacial Maximum to the Holocene. Proceedings of the National Academy of Sciences, 111(43), 15296-15303.

Le Maitre, R.W. 1984. A proposal by the IUGS Subcommission on the Systematics of Igneous Rocks for a chemical classification of volcanic rocks based on the total alkali silica (TAS) diagram: (on behalf of the IUGS Subcommission on the Systematics of Igneous Rocks). Australian Journal of Earth Sciences, 31(2), 243-255.

Lewis, K.B. 1973. Erosion and deposition on a tilting continental shelf during Quaternary oscillations of sea level. New Zealand journal of geology and geophysics, 16(2), 281-301.

Lewis, K.B. 1994. The 1500-km-long Hikurangi Channel: trench-axis channel that escapes its trench, crosses a plateau, and feeds a fan drift. Geo-Marine Letters, 14(1), 19-28.

Lewis, K.B., Barnes, P.M. 1999. Kaikoura Canyon, New Zealand: active conduit from near-shore sediment zones to trench-axis channel. Marine Geology, 162(1), 39-69.

Lewis, K.B., Pantin, H.M. 2002. Channel-axis, overbank and drift sediment waves in the southern Hikurangi Trough, New Zealand. Marine Geology, 192(1-3), 123-151.

Lewis, K.B., Pettinga, J.R. 1993. The emerging, imbricate frontal wedge of the Hikurangi margin. Sedimentary basins of the world, 2, 225-250.

Lewis, K.B., Collot, J.Y., Lallemand, S.E. 1998. The dammed Hikurangi Trough: a channel-fed trench blocked by subducting seamounts and their wake avalanches (New Zealand–France GeodyNZ Project). Basin Research, 10(4), 441-468.

Lewis, K.B., Lallemand, S.E., Carter, L. 2004. Collapse in a Quaternary shelf basin off East Cape, New Zealand: evidence for passage of a subducted seamount inboard of the Ruatoria giant avalanche. New Zealand Journal of Geology and Geophysics, 47(3), 415-429.

Lisiecki, L.E., Raymo, M.E. 2005. A Pliocene-Pleistocene stack of 57 globally distributed benthic δ18O records. Paleoceanography, 20(1).

Litchfield, N. 2003. Maps, Stratigraphic Logs and age Control Data for River Terraces in the Eastern North Island (IGNS Science Report 2003/31).

Litchfield, N.J., Berryman, K.R. 2005. Correlation of fluvial terraces within the Hikurangi Margin, New Zealand: implications for climate and baselevel controls. Geomorphology, 68(3-4), 291-313.

Litchfield, N.J., Berryman, K. 2006. Relations between postglacial fluvial incision rates and uplift rates in the North Island, New Zealand. Journal of Geophysical Research: Earth Surface, 111(F2).

Lorrey, A.M., Bostock, H. 2017. The climate of New Zealand through the Quaternary. In Landscape and Quaternary Environmental Change in New Zealand, 67-139. Atlantis Press, Paris.

Lougheed, B. C., Obrochta, S. P. 2019. A Rapid, Deterministic age-depth modeling routine for geological sequences with inherent depth uncertainty. Paleoceanography and Paleoclimatology, 34(1), 122-133

Lowe, D.J. 1988. Late Quaternary volcanism in New Zealand: towards an integrated record using distal airfall tephras in lakes and bogs. Journal of Quaternary science, 3(2), 111-120.

Lowe, D.R., Guy, M. 2000. Slurry-flow deposits in the Britannia Formation (Lower Cretaceous), North Sea: a new perspective on the turbidity current and debris flow problem. Sedimentology, 47(1), 31-70.

McArthur, A.D., McCaffrey, W.D. 2019. Sedimentary architecture of detached deep-marine canyons: Examples from the East Coast Basin of New Zealand. Sedimentology, 66(3), 1067-1101.

McArthur, A.D. Tek, D.E. 2021. Controls on the origin and evolution of deep-ocean trench-axial channels: Geology, 49, doi.org/10.1130/G48612.1.

McArthur, A.D., Claussmann, B., Bailleul, J., Clare, A., McCaffrey, W.D. 2020. Variation in syn-subduction sedimentation patterns from inner to outer portions of deep-water fold and thrust belts: examples from the Hikurangi subduction margin of New Zealand. Geological Society, London, Special Publications, 490(1), 285-310.

McCave, I. N. 1984a. Erosion, transport and deposition of fine-grained marine sediments. Geological Society, London, Special Publications 15.1, 35-69.

McCave, I. 1984b. Mechanics of deposition of fine-grained sediments from nepheloid layers. Geo-Marine Letters 4.3: 243-245.

McCave, I.N., Carter, L. 1997. Recent sedimentation beneath the Deep Western Boundary Current off northern New Zealand. Deep-Sea Research 44, 1203-1237.

McCave, I.N., Hall, I.R. 2006. Size sorting in marine muds: Processes, pitfalls, and prospects for paleoflow-speed proxies. Geochemistry, Geophysics, Geosystems, 7(10).

McCave, I.N., Carter, L., Hall, I.R. 2008. Glacial–interglacial changes in water mass structure and flow in the SW Pacific Ocean. Quaternary Science Reviews 27, 2008. 1886–1908.

McGlone, M.S. 2001. A late Quaternary pollen record from marine core P69, southeastern North Island, New Zealand. New Zealand Journal of Geology and Geophysics, 44(1), 69-77.

McGlone, M.S., Wilmshurst, J.M. 1999. Dating initial Maori environmental impact in New Zealand. Quaternary International, 59(1), 5-16.

McGlone, M.S., Salinger, M.J., Moar, N.T. 1993. Paleovegetation studies of New Zealand’s climate since the last glacial maximum. Global climates since the last glacial maximum, 294-317.

McGlone, M.S., Anderson, A.J., Holdaway, R.N. 1994. An ecological approach to the Polynesian settlement of New Zealand. The origins of the first New Zealanders, 136-163.

McNeill, L.C., Henstock, T.J. 2014. Forearc structure and morphology along the Sumatra-Andaman subduction zone. Tectonics, 33(2), 112-134.

McNeill, L.C., Dugan, B., Petronotis, K.E., Backman, J., Bourlange, S., Chemale, F., Chen, W., Colson, T.A., Frederik, M.C.G., Guèrin, G., Hamahashi, M., Henstock, T., House, B.M., Hüpers, A., Jeppson, T.N., Kachovich, S., Kenigsberg, A.R., Kuranaga, M., Kutterolf, S., Milliken, K.L., Mitchison, F.L., Mukoyoshi, H., Nair, N., Owari, S., Pickering, K.T., Pouderoux, H.F.A., Yehua, S., Song, I., Torres, M.E., Vannucchi, P., Vrolijk, P.J., Yang, T., and Zhao, X., 2017. Site U1480. In McNeill, L.C., Dugan, B., Petronotis, K.E., and the Expedition 362 Scientists, Sumatra Subduction Zone. Proceedings of the International Ocean Discovery Program, 362: College Station, TX (International Ocean Discovery Program). doi:10.14379/iodp.proc.362.103.2017

Mees, F., Swennen, R., Van Geet, M., Jacobs, P. 2003. Applications of X-ray computed tomography in the geosciences. Geological Society, London, Special Publications, 215(1), 1-6.

Migeon, S., Garibaldi, C., Ratzov, G., Schmidt, S., Collot, J.Y., Zaragosi, S., Texier, L. 2017. Earthquake-triggered deposits in the subduction trench of the north Ecuador/south Colombia margin and their implication for paleoseismology. Marine Geology, 384, 47-62.

Moore, M.I., Wilkin, J.L. 1998. Variability in the South Pacific Deep Western Boundary Current from current meter observations and a high-resolution global model. Journal of Geophysical Research: Oceans, 103(C3), 5439-5457.

Moore, J.C., Klaus, A., et al. 1998. Proceedings ODP, Initial Reports., 171A: College Station, TX (Ocean Drilling Program).

Moore, G.F., Taira, A., Klaus, A., et al. (eds.). 2001. Proceedings of the Ocean Drilling Program, 190 Initial Reports, Proceedings of the Ocean Drilling Program, 190, Ocean Drilling Program, 190, 1173-1178.

Mountjoy, J.J., Barnes, P.M. 2011. Active upper plate thrust faulting in regions of low plate interface coupling, repeated slow slip events, and coastal uplift: Example from the Hikurangi Margin, New Zealand. Geochemistry, Geophysics, Geosystems, 12(1).

Mountjoy, J.J., Barnes, P.M., Pettinga, J.R. 2009. Morphostructure and evolution of submarine canyons across an active margin: Cook Strait sector of the Hikurangi Margin, New Zealand. Marine Geology, 260(1-4), 45-68.

Mountjoy, J.J., Micallef, A., Stevens, C., Stirling, M. 2013, Holocene sedimentary activity in a non-terrestrially-coupled submarine canyon: Cook Strait, New Zealand: Deep-Sea Research Part II, 104, 120–133, doi:10.1016 /j.dsr2.2013.09.001.

Mountjoy, J.J., Howarth, J.D., Orpin, A.R., Barnes, P.M., Bowden, D.A., Rowden, A.A., Schimel, A.C., Holden, C., Horgan, H.J., Nodder, S.D., Patton, J.R. 2018. Earthquakes drive large-scale submarine canyon development and sediment supply to deep-ocean basins. Science advances, 4(3), p.eaar3748.

Mountjoy, J.J., Georgiopoulou, A., Chaytor, J., Clare, M.A., Gamboa, D., Moernaut, J. 2020. Subaqueous mass movements in the context of observations of contemporary slope failure. Geological Society, London, Special Publications, 500(1), 1-12.

Mulder, T., Syvitski, J.P., Migeon, S., Faugeres, J.C., Savoye, B. 2003. Marine hyperpycnal flows: initiation, behavior and related deposits. A review. Marine and Petroleum Geology, 20(6-8), 861-882.

Nelson, C.H. 1976. Late Pleistocene and Holocene depositional trends, processes, and history of Astoria deep-sea fan, northeast Pacific: Marine Geology, 20, 129–173.

Nelson, C. H., Goldfinger, C., Johnson, J. E., Dunhill, G. 2000a. Variation of Modem Turbidite Systems Along the Subduction Zone Margin of Cascadia Basin and Implications for Turbidite Reservoir Beds In book: Deep-water Reservoirs of the World: 20th Annual Research Conference, , p. Chapter: Variation of modern turbidite systems along the subduction zone margin of Cascadia Basin and implications for turbidite reservoir beds Publisher: Society of Economic Paleontologists and Mineralogists Editors: P.W. Weimer, R.M. Slatt, J. Coleman, N.C. Rosen, C.H. Nelson, A.H. Bouma, M.J. Styzen, D.T. Lawrence. 714-738

Nelson, C.S., Hendy, I.L., Neil, H.L., Hendy, C.H., Weaver, P.P.E. 2000b. Last glacial jetting of cold waters through the Subtropical Convergence zone in the Southwest Pacific off eastern New Zealand, and some geological implications.

Palaeogeography, Palaeoclimatology, Palaeoecology, 156(1-2), 103-121.

Newnham, R., McGlone, M., Moar, N., Wilmshurst, J., Vandergoes, M. 2013. The vegetation cover of New Zealand at the last glacial maximum. Quaternary Science Reviews, 74, 202-214.

Noda, A., Greve, A., Woodhouse, A., Crundwell, M. (Submitted). Depositional rate, grain size and magnetic mineral sulfidization in turbidite sequences, Hikurangi Margin, New Zealand. New Zealand Journal of Geology and Geophysics.

Orpin, A.R. 2004. Holocene sediment deposition on the Poverty-slope margin by the muddy Waipaoa River, East Coast New Zealand. Marine Geology, 209(1-4), 69-90.

Paterson, G.A., Heslop, D. 2015. New methods for unmixing sediment grain size data. Geochemistry, Geophysics, Geosystems, 16(12), 4494-4506.

Patton, J.R., Goldfinger, C., Morey, A.E., Ikehara, K., Romsos, C., Stoner, J., Djadjadihardja, Y., Udrekh, Ardhyastuti, S., Gaffar, E.Z., Vizcaino, A. 2015. A 6600 year earthquake history in the region of the 2004 Sumatra-Andaman subduction zone earthquake: Geosphere, 11(6), 1–63, doi:10.1130/GES01066.1.

Paquet, F., Proust, J.N., Barnes, P.M., Pettinga, J.R. 2009. Inner-forearc sequence architecture in response to climatic and tectonic forcing since 150 ka: Hawke's Bay, New Zealand. Journal of Sedimentary Research, 79(3), 97-124.

Paquet, F., Proust, J.N., Barnes, P.M., Pettinga, J.R. 2011. Controls on active forearc basin stratigraphy and sediment fluxes: The Pleistocene of Hawke Bay, New Zealand. GSA Bulletin, 123(5-6), 1074-1096.

Paull, C.K., McGann, M., Edwards, B.D., Barnes, P., Gwiazda, R., Lundsten, E.M., Anderson, K., Caress, D.W. 2014. Sub-decadal turbidite frequency during the early Holocene: Eel Fan, offshore northern California. Geology, 42: 10, 855-858, data Repository item 2014303, doi: 10. 1130/G35768.1

Pedley, K.L., Barnes, P.M., Pettinga, J.R., Lewis, K.B. 2010. Seafloor structural geomorphic evolution of the accretionary frontal wedge in response to seamount subduction, Poverty Indentation, New Zealand. Marine Geology, 270(1-4), 119-138.

Pickering, K.T., Pouderoux, H., McNeill, L.C., Backman, J., Chemale, F., Kutterolf, S., Milliken, K.L., Hideki, M., Henstock, T.J., Stevens, D.E., Parnell, C. 2020. Sedimentology, stratigraphy and architecture of the Nicobar Fan (Bengal–Nicobar Fan System), Indian Ocean: Results from International Ocean Discovery Program Expedition 362. Sedimentology.

Pillans, B., Chappell, J., Naish, T.R. 1998. A review of the Milankovitch climatic beat: template for Plio–Pleistocene sea-level changes and sequence stratigraphy. Sedimentary Geology, 122(1-4), 5-21.

Piper, D.W. 1978. Turbidite muds and silts on deepsea fans and abyssal plains. Sedimentation in submarine canyons, fans, and trenches.

Piper, D.J., von Huene, R., Duncan, J.R. 1973. Late Quaternary sedimentation in the active eastern Aleutian Trench. Geology, 1(1), 19-22.

Plaza-Faverola, A., Klaeschen, D., Barnes, P., Pecher, I., Henrys, S., Mountjoy, J. 2012. Evolution of fluid expulsion and concentrated hydrate zones across the southern Hikurangi subduction margin, New Zealand: An analysis from depth migrated seismic data. Geochemistry, Geophysics, Geosystems, 13(8).

Polonia, A., Panieri, G., Gasperini, L., Gasparotto, G., Bellucci, L.G., Torelli, L. 2013. Turbidite paleoseismology in the Calabrian Arc subduction complex (Ionian Sea). Geochemistry, Geophysics, Geosystems, 14(1), 112-140.

Postma, H. 1967. Sediment transport and sedimentation in the estuarine environment. American Association for the Advancement of Science, 83, 158–179.

Postma, G., Cartigny, M.J. 2014. Supercritical and subcritical turbidity currents and their deposits—A synthesis. Geology, 42(11), 987-990.

Pouderoux, H., Proust, J.N., Lamarche, G., Orpin, A., Neil, H. 2012a. Postglacial (after 18 ka) deep-sea sedimentation along the Hikurangi subduction margin (New Zealand): Characterisation, timing and origin of turbidites. Marine Geology, 295, 51-76.

Pouderoux, H., Proust, J.N., Lamarche, G., 2012b. Building an 18 000-year-long paleo-earthquake record from detailed deep-sea turbidite characterisation in Poverty Bay, New Zealand. Natural Hazards and Earth System Sciences, 12, 2077–2101. doi:10.5194/nhess-12-2077-2012.

Ratzov, G., Collot, J.Y., Sosson, M., Migeon, S. 2010. Mass-transport deposits in the northern Ecuador subduction trench: Result of frontal erosion over multiple seismic cycles. Earth and Planetary Science Letters, 296(1-2), 89-102.

Reeder, M.S., Stow, D.A., Rothwell, R.G. 2002. Late Quaternary turbidite input into the east Mediterranean basin: new radiocarbon constraints on climate and sea-level control. Geological Society, London, Special Publications, 191(1), 267-278.

Reilly, B. T., Stoner, J. S., Wiest, J. 2017. Sed CT: MATLAB™ tools for standardized and quantitative processing of sediment core computed tomography (CT) data collected using a medical CT scanner. Geochemistry, Geophysics, Geosystems, 18(8), 3231-3240.

Saffer, D.M., Wallace, L.M., Barnes, P.M., Pecher, I.A., Petronotis, K.E., LeVay, L.J., Bell, R.E., Crundwell, M.P., Engelmann de Oliveira, C.H., Fagereng, A., Fulton, P.M., Greve, A., Harris, R.N., Hashimoto, Y., Hüpers, A., Ikari, M.J., Ito, Y., Kitajima, H., Kutterolf, S., Lee, H., Li, X., Luo, M., Malie, P.R., Meneghini, F., Morgan, J.K., Noda, A., Rabinowitz, H.S., Savage, H.M., Shepherd, C.L., Shreedharan, S., Solomon, E.A., Underwood, M.B., Wang, M., Woodhouse, A.D., Bourlange, S.M., Brunet, M.M.Y., Cardona, S., Clennell, M.B., Cook, A.E., Dugan, B., Elger, J., Gamboa, D., Georgiopoulou, A., Han, S., Heeschen, K.U., Hu, G., Kim, G.Y., Koge, H., Machado, K.S., McNamara, D.D., Moore, G.F., Mountjoy, J.J., Nole, M.A., Owari, S., Paganoni, M., Rose, P.S., Screaton, E.J., Shankar, U., Torres, M.E., Wang, X., and Wu, H.-Y., 2019. Expedition 372B/375 summary. In Wallace, L.M., Saffer, D.M., Barnes, P.M., Pecher, I.A., Petronotis, K.E., LeVay, L.J., and the Expedition 372/375 Scientists, Hikurangi Subduction Margin Coring and Observatories. Proceedings of the International Ocean Discovery Program, 372B/375: College Station, TX (International

Ocean Discovery Program).

Schweller, W.J., Kulm, L.D. 1978. Extensional rupture of oceanic crust in the Chile Trench. Marine Geology, 28(3-4), 271-291.

Sclater, J.G., Christie, P.A. 1980. Continental stretching: An explanation of the post-Mid-Cretaceous subsidence of the central North Sea Basin. Journal of Geophysical Research: Solid Earth, 85(B7), 3711-3739.

Sexton, P.F., Wilson, P.A., Pearson, P.N. 2006. Microstructural and geochemical perspectives on planktic foraminiferal preservation: "Glassy" versus "Frosty". Geochemistry, Geophysics, Geosystems, 7(12).

Shephard, L.E., McMillen, K.J. 1981. Sedimentation rates of southwestern Mexico continental margin: DSDP Leg 66. In: Initial Reports of the Deep Sea Drilling Project. U.S. Government Printing Office, Washington, D.C., 66: 445-452

Shorrock, A. 2021. How have northern Hikurangi Margin gravity flow processes evolved in the past 42 ka? Insights from IODP Expedition 372B/375, Site U1520. (Master's thesis).

Smith, G., McNeill, L., Henstock, T.J., Bull, J. 2012. The structure and fault activity of the Makran accretionary prism. Journal of Geophysical Research: Solid Earth, 117(B7).

Soutter, E. L., Kane, I. A., Hodgson, D. M., Flint, S. 2021. The concavity of submarine canyon longitudinal profiles. Journal of Geophysical Research, Earth Surface, 126, e2021JF006185. https://doi.org/10.1029/2021JF006185.

Spratt, R.M., Lisiecki, L.E. 2016. A Late Pleistocene sea level stack. Climate of the Past, 12(4), 1079-1092.

Stanley, D.J., Knight, R.J., Stuckenrath, R., Catani, G. 1978. High sedimentation rates and variable dispersal patterns in the western Hellenic Trench. Nature, 273(5658), 110-113.

Stevens, C.L., O'Callaghan, J.M., Chiswell, S.M., Hadfield, M.G. 2021. Physical oceanography of New Zealand/Aotearoa shelf seas–a review. New Zealand Journal of Marine and Freshwater Research, 55(1), 6-45.

Stevenson, C.J., Talling, P.J., Masson, D.G., Sumner, E.J., Frenz, M., Wynn, R.B. 2014. The spatial and temporal distribution of grain-size breaks in turbidites. Sedimentology, 61(4), 1120-1156.

Stevenson, C.J., Jackson, C.A.L., Hodgson, D.M., Hubbard, S.M., Eggenhuisen, J.T. 2015. Deep-water sediment bypass. Journal of Sedimentary Research, 85(9), 1058-1081.

Stevenson, C.J., Peakall, J., Hodgson, D.M., Bell, D., Privat, A. 2020. TB or not TB: banding in turbidite sandstones. Journal of Sedimentary Research, 90(8), 821-842.

Stewart, R.B., Neall, V.E. 1984. Chronology of palaeoclimatic change at the end of the last glaciation. Nature, 311(5981), 47-48.

Stow, D.A., Shanmugam, G. 1980. Sequence of structures in fine-grained turbidites: comparison of recent deep-sea and ancient flysch sediments. Sedimentary Geology, 25(1-2), 23-42.

Stow, D.A.V., Piper, D.J.W. 1984. Deep-water fine-grained sediments: facies models. Geological Society, London, Special Publications, 15(1), 611-646.

Strachan, L.J., Bostock, H.C., Barnes, P.M., Neil, H.L., Gosling, M. 2016. Non-cohesive silt turbidity current flow processes; insights from proximal sandy-silt and silty-sand turbidites, Fiordland, New Zealand. Sedimentary Geology, 342, 118-132.

Su, X., Baumann, K.-H., Thiede, J. 2000. Calcareous nannofossils from Leg 168: biochronology and diagenesis, in Fisher, A.T., Davis, E.E., and Escutia, C., eds., Proceedings of the Ocean Drilling Program, Scientific Results, v. 168: College Station, Texas (Ocean Drilling Program), 39–50.

Sutton, P.J. 2003. The Southland Current: a subantarctic current. New Zealand Journal of Marine and Freshwater Research, 37(3), 645-652.

Taira, A., Niitsuma, N. 1985. Turbidite sedimentation in the Nankai Trough as interpreted from magnetic fabric, grain size, and detrital modal analyses, Initial Reports of the Deep Sea Drilling Project, 87, 611–632.

Talling, P.J., Masson, D.G., Sumner, E.J., Malgesini, G. 2012. Subaqueous sediment density flows: Depositional processes and deposit types. Sedimentology, 59(7), 1937-2003.

Tek, D.E., McArthur, A.D., Poyatos-Moré, M., Colombera, L., Patacci, M., Craven, B., McCaffrey, W.D. 2021a. Relating seafloor geomorphology to subsurface architecture: How mass-transport deposits and knickpoint-zones build the stratigraphy of the deep-water Hikurangi Channel. Sedimentology, 68(7), 3141-3190.

Tek, D.E., McArthur A.D., Poyatos-Moré M., Colombera L., Allen, C., Patacci, M., McCaffrey, W.D. 2021b. Controls on the architectural evolution of deep-water channel overbank sediment wave fields: insights from the Hikurangi Channel, offshore New Zealand, New Zealand Journal of Geology and Geophysics, doi: 10.1080/00288306.2021.1978509

Thornburg, T.M., Kulm, L.D. 1987. Sedimentation in the Chile Trench: Depositional morphologies, lithofacies, and stratigraphy. Geological Society of America Bulletin, 98(1), 33-52.

Thornburg, T.M., Kulm, L.D., Hussong, D.M. 1990. Submarine-fan development in the southern Chile Trench: a dynamic interplay of tectonics and sedimentation. Geological Society of America Bulletin, 102(12), 1658-1680.

Toucanne, S., Zaragosi, S., Bourillet, J.F., Naughton, F., Cremer, M., Eynaud, F., Dennielou, B. 2008. Activity of the turbidite levees of the Celtic–Armorican margin (Bay of Biscay) during the last 30,000 years: imprints of the last European deglaciation and Heinrich events. Marine Geology, 247(1-2), 84-103.

Turney, C.S., McGlone, M.S., Wilmshurst, J.M. 2003. Asynchronous climate change between New Zealand and the North Atlantic during the last deglaciation. Geology, 31(3), 223-226.

Underwood, M.B. 2007. Sediment inputs to subduction zones: Why lithostratigraphy and clay mineralogy matter. In Dixon, T.H., Moore, J.C. (eds.), The Seismogenic Zone of Subduction Thrust Faults. Columbia University Press, New York, 42-85.

Underwood, M.B., Karig, D.E. 1980. Role of submarine canyons in trench and trench slope sedimentation. Geology, 8, 432-436.

Underwood, M.B., Bachman, S.B. 1982. Sedimentary facies associations within subduction complexes. Geological Society, London, Special Publications, 10(1), 537-550.

Underwood, M.B., Moore, G.F. 1995. Trenches and slope basins, in Tectonics of Sedimentary basins, ed. C.J. Busby and R.V. Ingersoll, 179-219, Blackwell Sci., Malden, Mass.

Underwood, M.B., Pickering, K.T. 2018. Facies architecture, detrital provenance, and tectonic modulation of sedimentation in the Shikoku Basin: Inputs to the Nankai Trough subduction zone, in Byrne, T., Fisher, D., McNeill, L., Saffer, D., Ujiie, K., Underwood, M., Yamaguchi, A., (eds.), Geology and Tectonics of Subduction Zones: A Tribute to Gaku Kimura: Geological Society of America Special Paper 534, https://dx.doi.org/10.1130/2018.2534(XX).

Underwood, M.B., Orr, R., Pickering, K., Taira, A. 1993. Provenance and dispersal patterns of sediments in the turbidite wedge of Nankai Trough, in Hill, I.A., et al., eds., Proceedings of the Ocean Drilling Program, Scientific results, Volume 131: College Station, Texas, Ocean Drilling Program, 15–34, doi:10.2973/odp.proc.sr.131.105.1993.

Underwood, M.B., Hoke, K.D., Fisher, A.T., Davis, E.E., Giambalvo, E., Zühlsdorff, L., Spinelli, G.A., 2005. Provenance, stratigraphic architecture, and hydrogeologic influence of turbidites on the mid-ocean ridge flank of northwestern Cascadia Basin, Pacific Ocean. Journal of Sedimentary Research, 75(1), 149-164.

Upton, P., Kettner, A.J., Gomez, B., Orpin, A.R., Litchfield, N., Page, M.J. 2013. Simulating post-LGM riverine fluxes to the coastal zone: The Waipaoa River System, New Zealand. Computers & Geosciences, 53, 48-57.

Vandekerkhove, E., Van Daele, M., Praet, N., Cnudde, V., Haeussler, P. J., De Batist, M. 2020. Flood-triggered versus earthquake-triggered turbidites: A sedimentological study in clastic lake sediments (Eklutna Lake, Alaska). Sedimentology, 67(1), 364-389.

Völker, D., Wiedicke, M., Ladage, S., Gaedicke, C., Reichert, C., Rauch, K., Kramer,W., Heubeck, C. 2006. Latitudinal variations in sedimentary processes in the Peru-Chile trench off Central Chile. In: Oncken, G.C.O., Franz, G., Giese, P., Götze, H.-J., Ramos, V.A., Strecker, M.R., Wigger, P. (Eds.), The Andes—Active Subduction Orogeny. Springer-Verlag, 193–216.

von der Borch, C.C., Sclater, J.G., Gartner, S.Jr., Hekinian, R., Johnson, D.A., McGowran, B., Pimm, A.C., Thompson, R.W., Veevers, J.J., Waterman, L.S. 1974. Site 211. Texas A&M University, Ocean Drilling Program, College Station, TX, United States, In: von der Borch, C.C., Sclater, J.G., Gartner, S.Jr., Hekinian, R., Johnson, D.A., McGowran, B., Thompson, R.W., Veevers, J.J., Waterman, L.S., Pimm, A.C. (eds.), Initial reports of the Deep Sea Drilling Project, covering Leg 22 of the cruises of the drilling vessel Glomar Challenger; Darwin, Australia to Colombo, Ceylon, January-March 1972, 22, 13-36, georefid:1983-030636

von Huene, R. 1974. Modern Trench Sediments. In: Burk C.A., Drake C.L. (eds.), The Geology of Continental Margins. Springer, Berlin, Heidelberg. https://doi.org/10.1007/978-3-662-01141-6_15

von Huene, R., Kulm, L.D. 1973. Tectonic summary of Leg 18, in Kulm, L.D., and von Huene, R., eds., Initial Reports Deep Sea Drilling Project: Washington, D.C., U.S. Government Printing Office, 961–976

Wallace, L.M., Beavan, J., McCaffrey, R., Darby, D. 2004. Subduction zone coupling and tectonic block rotations in the North Island, New Zealand. Journal of Geophysical Research: Solid Earth, 109(B12).

Wallace, L.M., Reyners, M., Cochran, U., Bannister, S., Barnes, P.M., Berryman, K., Downes, G., Eberhart-Phillips, D., Fagereng, A., Ellis, S., Nicol, A., 2009. Characterizing the seismogenic zone of a major plate boundary subduction thrust:

Hikurangi Margin, New Zealand. Geochemistry, Geophysics, Geosystems, 10(10).

Wallace, L.M., Saffer, D.M., Barnes, P.M., Pecher, I.A., Petronotis, K.E., LeVay, L.J., Bell, R.E., Crundwell, M.P., Engelmann de Oliveira, C.H., Fagereng, A., Fulton, P.M., Greve, A., Harris, R.N., Hashimoto, Y., Hüpers, A., Ikari, M.J., Ito, Y., Kitajima, H., Kutterolf, S., Lee, H., Li, X., Luo, M., Malie, P.R., Meneghini, F., Morgan, J.K., Noda, A., Rabinowitz, H.S., Savage, H.M., Shepherd, C.L., Shreedharan, S., Solomon, E.A., Underwood, M.B., Wang, M., Woodhouse, A.D., Bourlange, S.M., Brunet, M.M.Y., Cardona, S., Clennell, M.B., Cook, A.E., Dugan, B., Elger, J., Gamboa, D., Georgiopoulou, A., Han, S., Heeschen, K.U., Hu, G., Kim, G.Y., Koge, H., Machado, K.S., McNamara, D.D., Moore, G.F., Mountjoy, J.J., Nole, M.A., Owari, S., Paganoni, M., Rose, P.S., Screaton, E.J., Shankar, U., Torres, M.E., Wang, X., Wu, H.-Y. 2019a. Expedition 372B/375 methods. In Wallace, L.M., Saffer, D.M., Barnes, P.M., Pecher, I.A., Petronotis, K.E., LeVay, L.J., and the Expedition 372/375 Scientists, Hikurangi Subduction Margin Coring, Logging, and Observatories. Proceedings of the International Ocean Discovery Program, 372B/375: College Station, TX (International Ocean Discovery Program).

Wallace, L.M., Saffer, D.M., Petronotis, K.E., Barnes, P.M., Bell, R.E., Crundwell, M.P., Engelmann de Oliveira, C.H., Fagereng, A., Fulton, P.M., Greve, A., Harris, R.N., Hashimoto, Y., Hüpers, A., Ikari, M.J., Ito, Y., Kitajima, H., Kutterolf, S., Lee, H., Xuesen, L., Min, L., Malie, P.R., Meneghini, F., Morgan, J.K., Noda, A., Rabinowitz, H.S., Savage, H.M., Shepherd, C.L., Shreedharan, S., Solomon, E.A., Underwood, M.B., Maomao, W., and Woodhouse, A.D., 2019b. Site U1526. In Wallace, L.M., Saffer, D.M., Barnes, P.M., Pecher, I.A., Petronotis, K.E., LeVay, L.J., and the Expedition 372/375 Scientists (Ed.), Hikurangi Subduction Margin Coring, Logging, and Observatories. Proceedings of the International Ocean Discovery Program, 372B/375: College Station, TX (International Ocean Discovery Program).

Watson, S.J., Mountjoy, J.J., Crutchley, G.J. 2020. Tectonic and geomorphic controls on the distribution of submarine landslides across active and passive margins, eastern

New Zealand. Geological Society, London, Special Publications, 500(1), 477-494.

Westbrook, G.K., Mascle, A., Biju-Duval, B. 1984. Geophysics and the structure of the Lesser Antilles forearc. Initial Reports Deep Sea Drilling Program, LXXVIIIA, 23-38.

Westbrook, G. K., et al. 1994. Proceedings of the Ocean Drilling Program, Initial Reports, vol. 146, Ocean Drilling Program, College Station, Texas.

Wetzel, A., Balson, P. 1992. Sedimentology of fine-grained turbidites inferred from continuously recorded physical properties data. Marine Geology, 104(1-4), 165-178.

Whitworth III, T., Warren, B.A., Nowlin Jr, W.D., Rutz, S.B., Pillsbury, R.D., Moore, M.I. 1999. On the deep western-boundary current in the Southwest Pacific Basin. Progress in Oceanography, 43(1), 1-54.

Williams, P.W., McGlone, M., Neil, H., Zhao, J.X. 2015. A review of New Zealand palaeoclimate from the Last Interglacial to the global Last Glacial Maximum. Quaternary Science Reviews, 110, 92-106.

Wright, A. 1984. Sediment accumulation rates of the Lesser Antilles intraoceanic island arc. In: Moore, J. C., Biju-Duval, B., et al., Initial Reports of the Deep Sea Drilling Project, Volume 78:357-368. Washington, D.C., U.S. Government Printing Office

Yang, Y., Gao, S., Ping Wang, Y., Jia, J., Xiong, J., Zhou, L. 2019. Revisiting the problem of sediment motion threshold. Continental Shelf Research, 187.

Zuffa, G.G., Normark, W.R., Serra, F., Brunner, C.A. 2000. Turbidite megabeds in an oceanic rift valley recording jökulhlaups of late Pleistocene glacial lakes of the western United States. The Journal of Geology, 108(3), 253-274.

Sample ID	Core	Sampling range (m)		^{14}C age (yr)	2σ error (yr)	Cal. age (median in yr BP)	2σ range (cal. yr)
		Upper	Lower				
NZA68060	1H4W	5.21	5.29	8464	38	8695	8452 – 8966
NZA68061	2H1W	6.48	6.56	10,085	45	10,828	10,549 – 10,995
NZA68062	2H4W	10.82	10.9	13,513	67	15,283	14,973 – 15,607
NZA68063	4H6W	33.01	33.05	17,148	105	19,650	19,267 – 20,046
NZA68790	6H4W	49.095	49.145	18,532	124	21,347	20,902 – 21,811
NZA68791	7H3W	57.08	57.12	20,944	168	24,038	23,647 – 24,565
NZA69011	11H4W	96.2	96.26	25,652	328	28,901	28,154 – 29,722
NZA69516	12HCC	106.2	106.32	39,185	1679	42,440	39,932 – 45,971

Table 1. Radiocarbon datums used to construct the U1520 age model.

Core	Sampling range (m)		Tephra	Cal. age (median in yr BP)	2σ error (cal. yr)
	Upper	Lower			
1H1A	1.19	1.21	Taupo	1718	10
1H3A	3.17	3.33	Waimihia	3382	50
1H3A	3.7	3.72	Whakatane	5542	48
1H4A	5.41	5.44	Rotoma	9472	40
2H1A	6.12	6.17	Opepe	10,004	122

Table 2. Primary tephra datums and depths used to construct the U1520 age model.

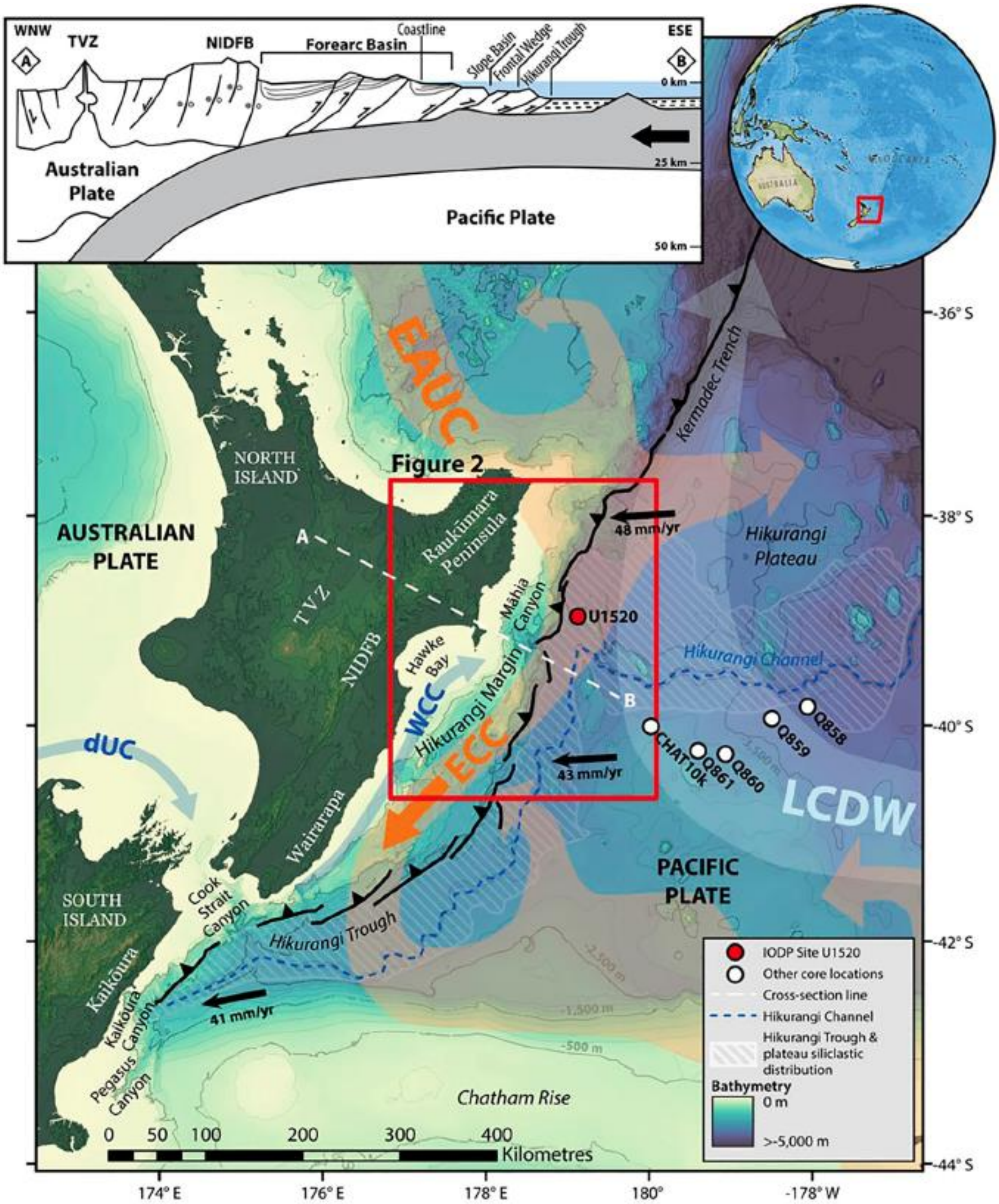

Figure 1. Map and cross section of the Hikurangi Subduction Margin. TVZ = Taupo Volcanic Zone, NIDFB = North Island Dextral Fault Belt. Adapted from Lewis et al. (1998), Barnes et al. (2010), and Pedley et al. (2010). Shaded pink polygon with orange arrows denote the East Auckland Current (EAUC) and East Cape Current (ECC). Grey arrows denote D'urville Current (dUC) and Wairarapa Coastal Current (WCC). Light grey polygon with northward arrow denotes the Lower Circumpolar Deep Waters

(LCDW), part of the Deep Western Boundary Current. Bold black arrows are relative Pacific-Australian plate motion rates.

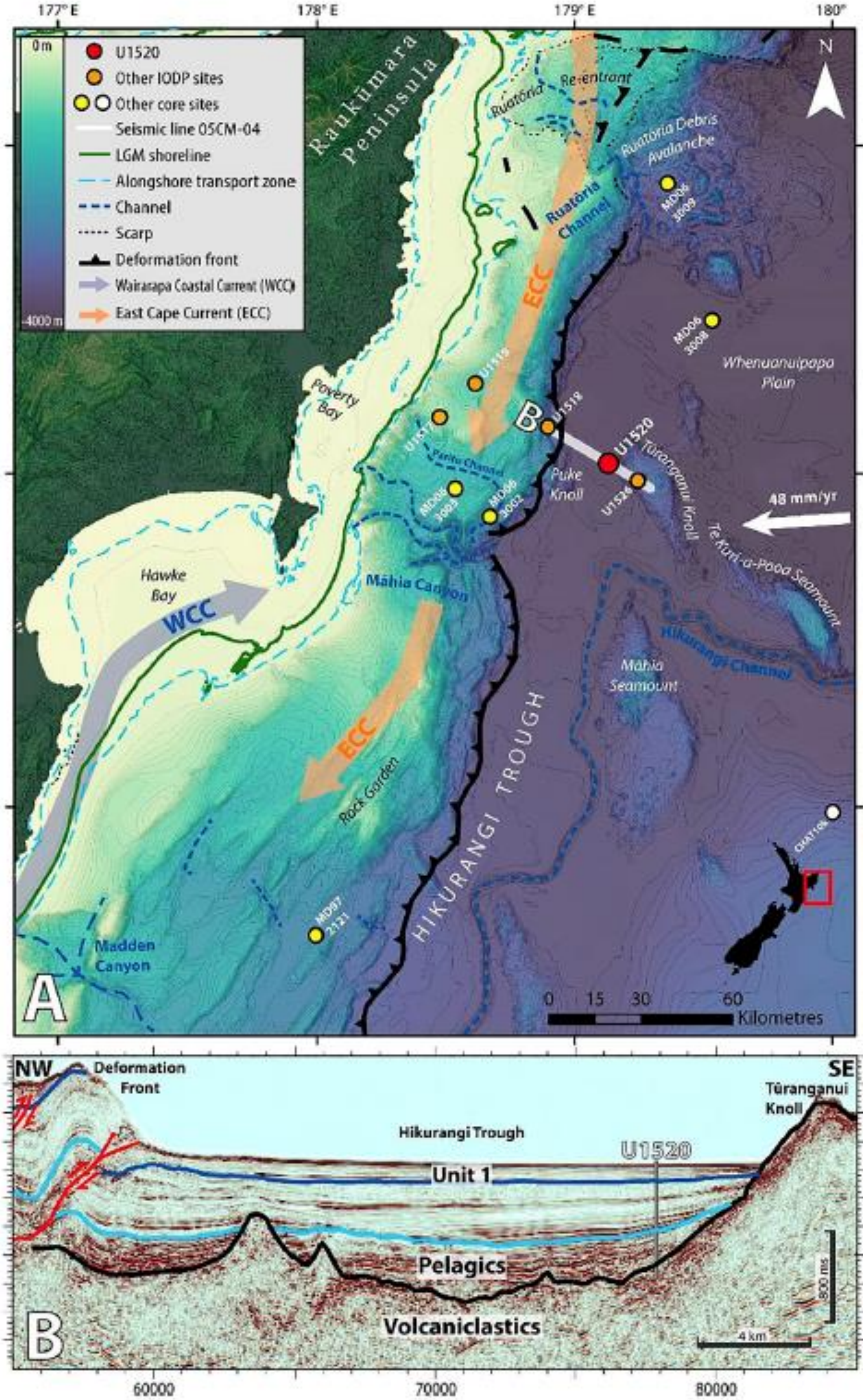

Figure 2. A. Regional bathymetric map of north eastern HSM showing major canyons

and channels, surface-circulation oceanographic currents, IODP Expedition 372-375 sites, and Marion Dufresne core locations denoted by MD. LGM = Last Glacial Maximum. B. Regional seismic section 05CM-04 (Bell et al. 2010; Barker et al. 2018; Barnes et al. 2020) crossing the northern Hikurangi Trough over IODP Site U1520, showing the distribution of the studied Unit I sequence and other major lithological horizons.

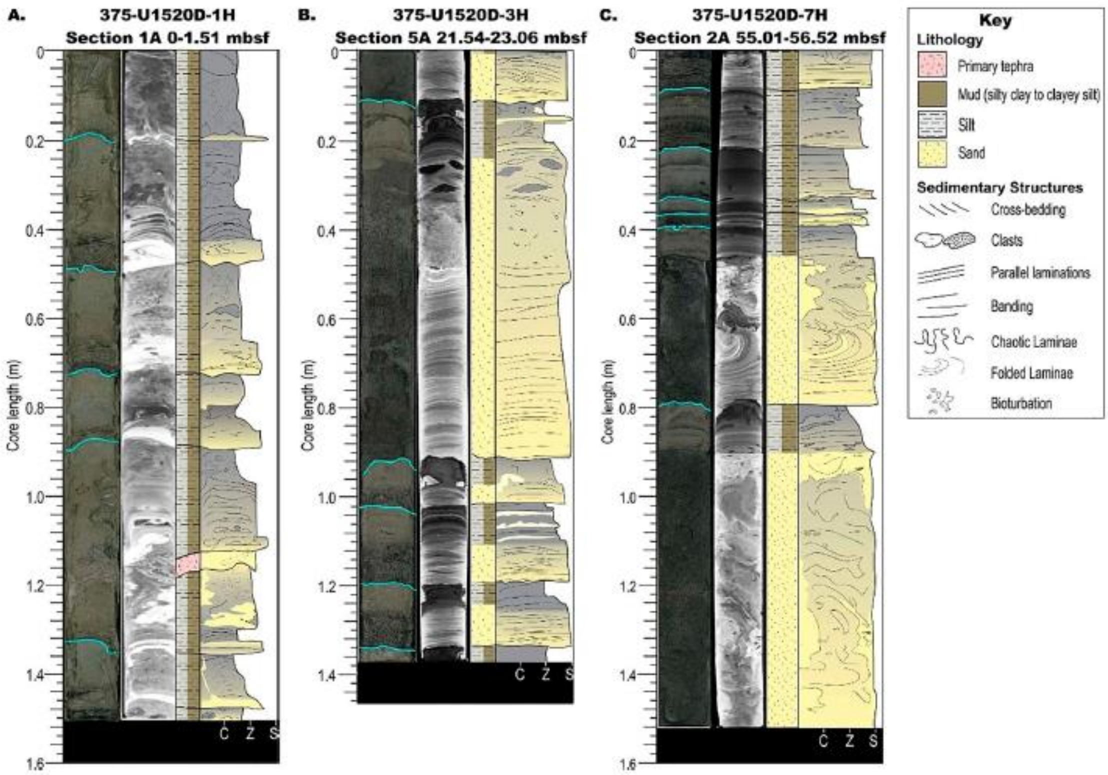

Figure 3. Example core photographs. CT scans and sedimentary logs from cores A. 375-U1520D-1H-1A from 0-1.51 mbsf, B. 375-U1520D-3H-5A from 21.53-23.06 mbsf, and C. 375-U1520D-7H-2A from 55.01-56.52 mbsf. Bed boundaries are highlighted on core photographs as blue lines.

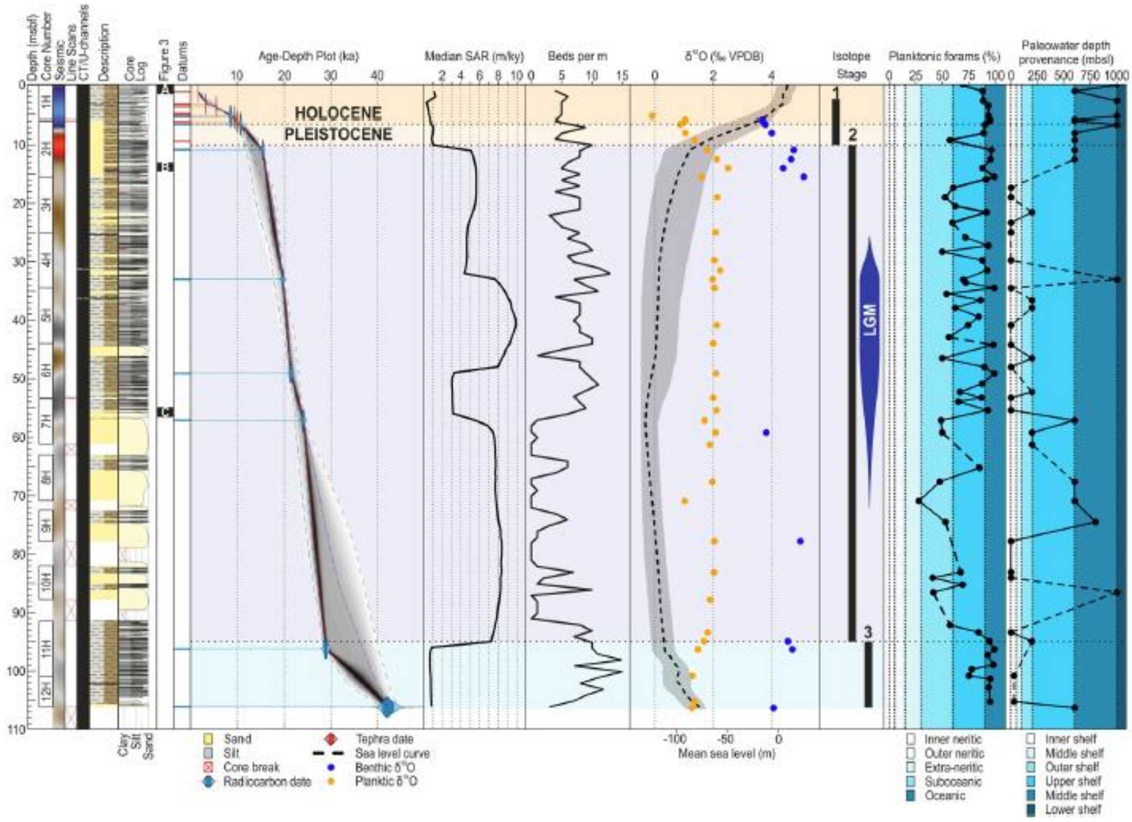

Figure 4. Log of lithology showing CT scanned intervals, u-channel intervals, AMS-^{14}C dates, tephras, age-depth, sedimentation rates, beds per metre, stable isotopes with interpreted LGM (Lorrey and Bostock, 2017), relative sea level (Spratt and Lisiecki, 2016), isotope stages (Lisiecki and Raymo, 2005), % planktonic foraminifera as an indicator of oceanicity (Hayward et al. 1999), and paleo-water depth from benthic foraminifera indicator species (Hayward et al. 2019).

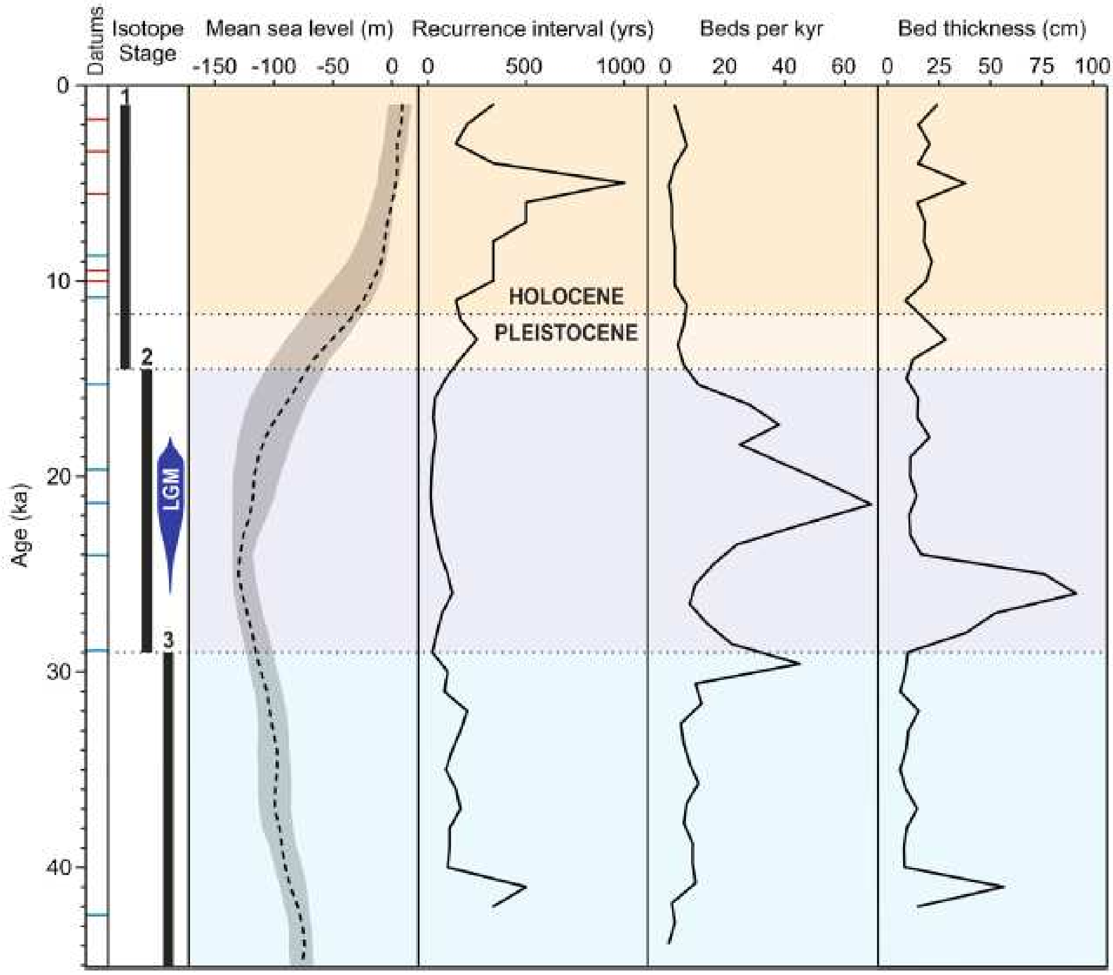

Figure 5. Log of marine isotopes stages, relative sea level (Spratt and Lisiecki, 2016), bed recurrence interval (RI), beds per kyr, and bed thickness (cm). LGM = last glacial maximum, datum colours, red = tephra, blue = AMS-^{14}C.

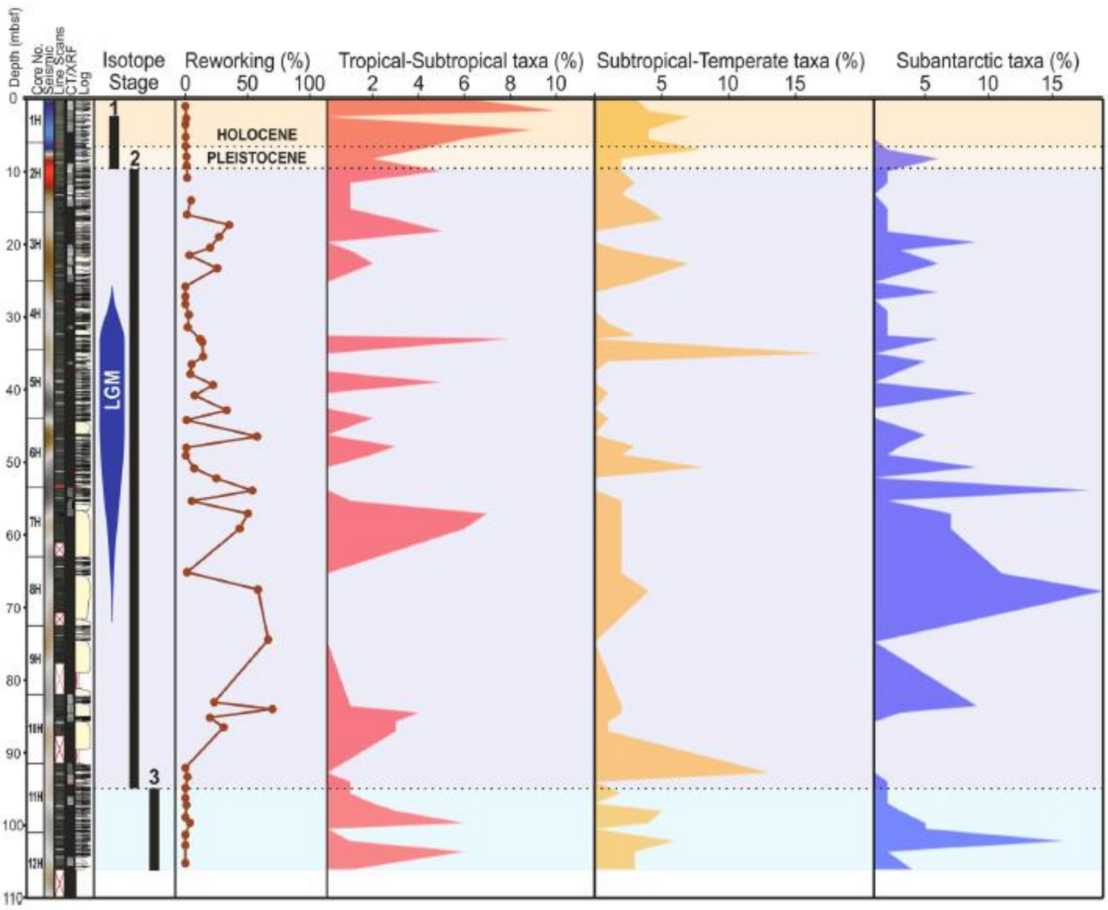

Figure 6. Log of down-core MIS and LGM extent, % Miocene/Pliocene reworking, and abundance profiles of selected planktonic foraminiferal assemblage categories of Crundwell et al. (2008) in Unit I.

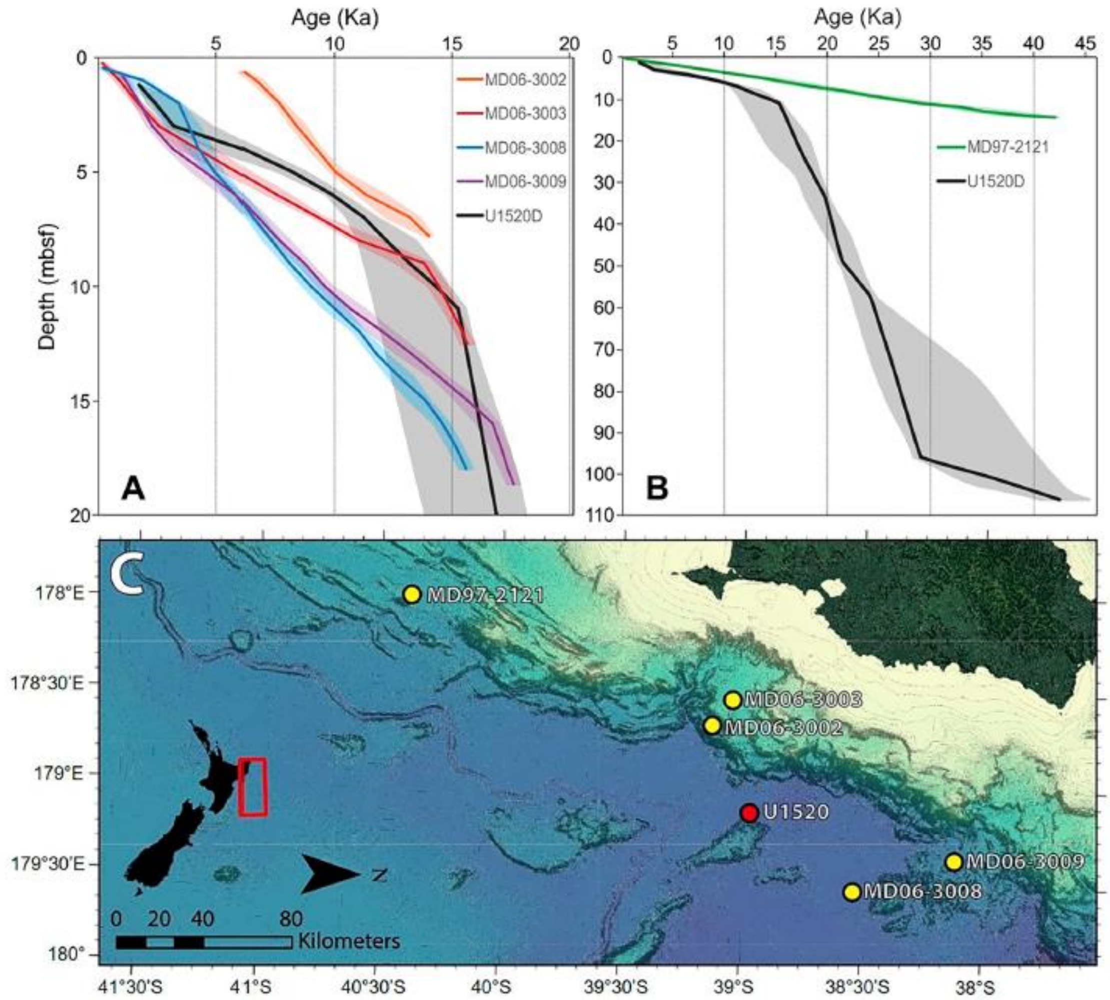

Figure 7. Comparative age-depth plots of A. sites U1520D, MD06-3002, MD06-3003, MD06-3008, and MD06-3009, and B. sites U1520D and MD97-2121. Data from this study and Pouderoux et al. (2012a).

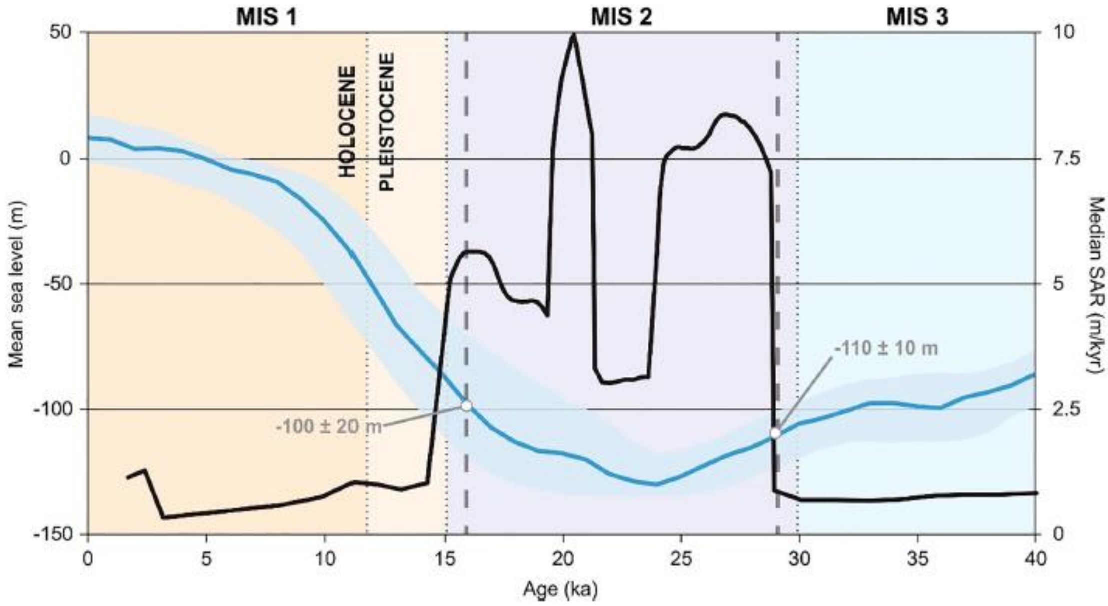

Figure 8. Comparative plot of relative sea level (Spratt and Lisiecki, 2016) and sediment accumulation rate demonstrating the possible positioning of the regional sea level threshold (modified from Shorrock, 2021).